Research Square

Preprints are preliminary reports that have not undergone peer review.
They should not be considered conclusive, used to inform clinical practice,
or referenced by the media as validated information.

An oncolytic reovirus-based platform amenable to oral vaccination

Salar Pashangzadeh
CHEO Research Institute
Xiao Xiang
Key Laboratory of Biorheological Science and Technology (Chongqing University)
Nikolas Martin
CHEO Research Institute
Yang Long
Key Laboratory of Biorheological Science and Technology (Chongqing University)
Ki-Hoon Song
ViroCure, #502, Ace TwinTower 1, 285 Digital-ro, Guro-gu, Seoul 08381, Republic of Korea
Negar Sharifi
CHEO Research Institute
Eknoor Walia
CHEO Research Institute
Serana Topshee
CHEO Research Institute
Mariam Maltseva
University of Ottawa
Kyle Malone
CHEO Research Institute
Carlos Giraldo
CHEO Research Institute
An-Dao Yang
CHEO Research Institute
Thet Fatica
CHEO Research Institute
Julia Petryk
Ottawa Hospital Research Institute
Nathalie Earl
CHEO Research Institute
Marc-Andre Langlois
University of Ottawa
Guy Lemay

Université de Montreal

Young-Kwan Lee
ViroCure, #502, Ace TwinTower 1, 285 Digital-ro, Guro-gu, Seoul 08381, Republic of Korea

Huy-Dung Hoang
CHEO Research Institute

Jiahu Wang
Genvira Biosciences

Kensuke Hirasawa
Memorial University of Newfoundland

John Bell
Ottawa Hospital Research Institute https://orcid.org/0000-0002-9083-357X

Wang-Jun Lee
ViroCure, #502, Ace TwinTower 1, 285 Digital-ro, Guro-gu, Seoul 08381, Republic of Korea

Shawn Beug
CHEO Research Institute

Tommy Alain
tommy@arc.cheo.ca

CHEO Research Institute, University of Ottawa https://orcid.org/0000-0002-0396-9138

Article

Keywords: Reovirus, Oncolytic Virus, Oral Vaccination, Mucosal Immunity, Cancer Vaccine

Posted Date: September 8th, 2026

DOI: https://doi.org/10.21203/rs.3.rs-9956033/v1

License: This work is licensed under a Creative Commons Attribution 4.0 International License.
Read Full License

Additional Declarations: There is a conflict of interest K-H.S., Y-K. L. and W-J. L are affiliated with ViroCure Inc. T.A. and X.X. have a consulting and advisory role at ViroCure, CuroV Science and Genvira Biosciences. The other authors declared no conflict of interest related to this work.

An oncolytic reovirus-based platform amenable to oral vaccination

Salar Pashangzadeh[1,2,#], Xiao Xiang[1,2,3,4,#,*], Nikolas T. Martin[2], Yang Long[3,4], Ki-Hoon Song[5], Negar Sharifi[1,2], Eknoor Walia[1,2], Serena Topshee[2], Mariam Maltseva[1], Kyle Malone[1,2], Carlos Rios Giraldo[2], An-Dao Yang[2], Thet Fatica[2], Julia Petryk[6], Nathalie Earl[2], Marc-André Langlois[1], Guy Lemay[7], Young-Kwan Lee[5], Huy-Dung Hoang[2], Jiahu Wang[8], Kensuke Hirasawa[9], John C. Bell[1,6], Wang-Jun Lee[5], Shawn T. Beug[1,2,10], Tommy Alain[1,2,10,*]

Affiliations:

[1] Department of Biochemistry, Microbiology and Immunology, Faculty of Medicine, University of Ottawa, Ottawa, ON, Canada

[2] Children's Hospital of Eastern Ontario Research Institute, Ottawa, ON, Canada

[3] College of Bioengineering, Chongqing University, Chongqing 400044, China

[4] Key Laboratory of Biorheological Science and Technology (Chongqing University), Ministry of Education, Chongqing 400044, China

[5] ViroCure, #502, Ace TwinTower 1, 285 Digital-ro, Guro-gu, Seoul 08381, Republic of Korea

[6] Ottawa Hospital Research Institute, Ottawa, ON, Canada

[7] Département de microbiologie, infectiologie et immunologie, Faculté de médecine, Université de Montréal, Montréal, QC, Canada

[8] Genvira Biosciences, Ottawa, ON, Canada

[9] Division of BioMedical Sciences, Memorial University of Newfoundland, St. John's, Newfoundland, Canada

[10] Centre for Infection, Immunity and Inflammation, Faculty of Medicine, University of Ottawa, Ottawa, ON, Canada

[#]These authors contributed equally.

[*]**Corresponding Authors:**

Xiao Xiang, PhD

College of Bioengineering, Chongqing University, Chongqing 400044, China

Key Laboratory of Biorheological Science and Technology (Chongqing University), Ministry of Education, Chongqing 400044, China

Email Address: xiaoxiang_bioeng@cqu.edu.cn

Tommy Alain, PhD

Department of Biochemistry, Microbiology and Immunology, Faculty of Medicine, University of Ottawa, ON, Canada

Email Address: tommy@arc.cheo.ca

Running title: Reovirus as a multi-route vaccine platform

Keywords: Reovirus, Oncolytic Virus, Oral Vaccination, Mucosal Immunity, Cancer Vaccine

Abstract

A major challenge in vaccine development is achieving durable systemic and mucosal immunity through non-invasive delivery while maintaining safety and tolerability. Here, we introduce a live-attenuated Reovirus Type 3 Dearing (T3D) platform that elicits robust immune responses when delivered by multiple delivery routes, particularly oral administration. By replacing the JAM-A binding domain of the σ1 attachment protein with structurally diverse antigens, including ovalbumin (OVA) and the receptor-binding domain (RBD) of SARS-CoV-2, we created a vaccination platform with intrinsic adjuvanticity and safety. All administration routes elicited potent antigen-specific $CD8^+$ T-cell and IgG responses, whereas oral delivery uniquely triggered robust mucosal IgA production. Recombinant reovirus displaying linear and conformational SARS-CoV-2 epitopes induced systemic and mucosal neutralizing antibodies, underscoring the platform's potential for infection control. Administration via conventional routes abolished tumour engraftment and suppressed its growth in a B16F10-OVA melanoma model, while oral delivery showed drastic inhibition of melanoma metastasis to the lungs and synergized with immune checkpoint blockers, demonstrating strong prophylactic and therapeutic efficacy. Together, our findings position attenuated reovirus as a first-in-class, tunable oral vaccine platform for infectious diseases and cancer.

Introduction

The global burden of infectious diseases and cancer necessitates the development of innovative vaccination platforms that elicit comprehensive immune responses [1, 2]. Effective vaccines must overcome several obstacles, including efficient antigen presentation, durability of immune responses, and mode of delivery. Unfortunately, antigen delivery remains one of the most significant challenges in modern vaccine development. While most licensed vaccines rely on intramuscular (IM) or subcutaneous (SC) injections, these routes primarily stimulate systemic immunity and often fail to induce robust responses at mucosal surfaces, which often are primary entry sites for many pathogens, such as coronaviruses, and location of highly prevalent malignancies, including lung and colorectal cancer [3, 4]. Moreover, vaccines often require trained personnel, cold-chain storage, and compliance with needle-based delivery, which pose logistical challenges, especially in resource-limited settings or low-income countries [4].

Oral vaccination represents a particularly attractive solution due to its ease of administration, patient compliance, and ability to engage both the systemic and mucosal immune systems [5, 6]. By targeting gut-associated lymphoid tissues (GALT), oral vaccines stimulate secretory IgA and mucosal T cell responses, offering a first line of defense at the site of pathogen entry or tumour development [3, 7]. However, translating this approach has proven challenging. Oral vaccines must contend with harsh gastrointestinal (GI) conditions, including acidic pH and proteolytic enzymes, as well as physiological barriers that limit antigen uptake and immune priming [8, 9]. Despite these obstacles, a platform that can withstand the GI environment while delivering immunogenic payloads to mucosal inductive sites would represent a major advancement for both infectious disease and cancer immunoprevention.

Reovirus Type 3 Dearing (T3D) is a double-stranded RNA virus that naturally infects the host through the enteric route and possesses several features that make it well-suited for oral vaccine development. Upon ingestion, reovirus particles are proteolytically processed into intermediate subviral particles (ISVPs) by intestinal enzymes or endosomal cathepsins, facilitating entry into epithelial cells via receptors such as sialic acid (SA) and junctional adhesion molecule A (JAM-A) [10-13]. The microfold cells within the intestinal epithelium transport reovirus to Peyer's patches, where antigen-presenting cells initiate adaptive immune responses. From there, activated lymphocytes can disseminate through the mesenteric lymph nodes and thoracic duct to establish systemic immunity. However, reovirus can replicate in multiple regions of the gut, including the ileum, jejunum, and colon [14]. Unlike many experimental oral vectors, reovirus is intrinsically stable in acidic environments and shows a natural tropism for GALT, allowing it to seed mucosal inductive sites without requiring artificial encapsulation or high-dose administration [15]. Currently, reovirus has been extensively studied in clinical trials as an oncolytic agent, with delivery via intravenous (IV) and intratumoural (IT) routes. These trials have demonstrated its safety and immunogenicity in humans, further supporting its use as a vaccine platform [16].

In our prior work, we developed and characterized two reovirus variants, namely RC402 and RP116, as therapeutic agents [14, 17, 18]. RC402 was a T3D wildtype variant isolated in South Korea and is being developed into oncolytics. This variant selectively infects tumour cells while sparing normal tissues, and when administered orally, RC402 robustly induces durable $CD8^+$ T cell immunity in both orthotopic and spontaneous mouse colorectal cancer models [14]. In follow-

up studies, we show that RP116, a previously discovered reovirus mutant with a truncated σ1 protein that lacks the JAM-A-binding domain, retains potent oncolytic activity and synergizes with immune checkpoint blockade to eliminate tumours and prevent relapse [17]. Interestingly, RP116 was more resistant to repeated delivery compared to RC402 as it lacked the immune-dominant JAM-A domain. Thus, these studies position reovirus as an ideal vector for oral and systemic delivery of epitopes.

In this study, we engineered a reovirus T3D-based vaccine by replacing the JAM-A-binding globular head of the σ1 protein with a range of antigens, including the receptor-binding domain (RBD) of SARS-CoV-2, the model antigen ovalbumin (OVA), ADP-dependent glucokinase (Adpgk), and Ribosomal Protein L18 (Rpl18). These constructs were designed to elicit robust immune responses by leveraging the natural immunogenicity of replication competent reovirus. Importantly, we investigated the feasibility of delivering this vaccine via oral administration, as well as intraperitoneal (IP) injection, to evaluate its potential for stimulating both systemic and mucosal immunity. Using a B16F10-OVA melanoma mouse model, we demonstrate that the vaccine prevents tumour formation and inhibits tumour progression following both orally (PO) and IP administration. Oral delivery uniquely stimulated mucosal immunity, evidenced by antigen-specific IgA production and activation of GALT even with previous exposures of the wild-type (WT) reovirus. These findings establish recombinant reovirus T3D as a versatile platform for developing vaccines against infectious diseases and cancer, with the added advantage of needle-free oral delivery to improve accessibility.

Results

Replication competent reovirus can be engineered to display and encode immunogenic epitopes.

The goal of this study was to develop a recombinant reovirus (ReoV) encoding immunogenic epitopes [19, 20], originating from infectious diseases severe acute respiratory syndrome coronavirus 2 (SARS-CoV-2) or tumour antigens (e.g., Adpgk, Rpl18) that is stable, replication competent, safe, and immunogenic upon oral administration We have developed an optimized cloning (**Figure S1A, B**) and rescue pipeline for the generation of recombinant ReoV serotype T3D based on plasmid-based reverse genetics system [21]. A naturally occurring ReoV variant (ReoV-Q251*, RP116) with a premature STOP codon in the *S1* gene [17] allowed for insertion of 615 bp (205 aa), at the 3' end of the *S1*. We cloned the cds of different antigens (SARS-CoV-2 RBD, S21P2) or epitopes (OVA, $OVA^{323-339}$/OVA CD4, Adpgk, Rpl18) fused to 5' sequence of *S1* by a glycine-serine linker and flanked on the 5' end by the cds for a Myc tag and at the 3' end by the cds for a FLAG tag. This strategy replaces the virus head domain with the newly introduced epitopes, while persevering SA binding site (**Figure 1A, left**). **Figure 1A, right** depicts protein structures (crystal structure for σ1-WT and based on that for σ1-Q251* (pdb_00003s6z), AlphaFold 3 predictions for σ1-RBD and σ1-OVA) of the C-terminal portion of the σ1 protein of different ReoV variants, highlighting the considerable size differences. Proper assembly of recombinant virus particles was then demonstrated after 3-4 passages of the virus in cell culture supernatant from infected cells by immunoblotting against either all ReoV proteins using a ReoV T3D antiserum (rabbit) or the Myc tag linking the N-terminal tail of σ1 to the recombinant C-

terminal region comprising the introduced antigens or epitopes, respectively. Expression of the recombinant σ1-fusion proteins can be detected at varying apparent molecular weights ranging from 25 – 48 kDa. Additionally, transcription and propagation of the recombinant S1 gene was demonstrated after 3-4 passages of the virus by PCR on cDNA generated from bulk RNA from infected cells using a primer pair binding within the cds of the N-terminal tail of σ1, yielding a product of approx. 200 bp (lower gel) or a primer pair binding in both the tail domain and in the cds for the T cell epitopes, yielding a product of approx. 650 bp (upper gel) (**Figure 1B-D**). Recombinant viruses also display remarkable genomic integrity over several passages as the flanking FLAG and Myc tags can be detected by immunoblotting after 12 and 13 passages of ReoV-OVA and ReoV-S21P2, respectively, of the on L929 cells (**Figure S1C**). Sequencing of the S1 gene after 12 to 13 passages shows only three mutations (**Figure S1D**), of these only 2 are non-synonymous (N197D, K265N). Of note, N197D is in close proximity to the SA binding site and might be involved in binding this receptor. We also show the presence and colocalization of bulk ReoV proteins (green, first and second row), the absence (WT, ReoV-Q251*, ReoV-RBD) and presence (ReoV-S21P2, ReoV-OVA) of recombinant σ1-fusion proteins (red, first and third row) in the cytosol of cells infected with the indicated virus variants using immunofluorescent staining (**Figure 1E**).

Viral growth kinetics over the first 48 hours post-infection (hpi) showed that while recombinant variants replicated slightly more efficiently at 12 hpi (see inset), total titers at 48 hpi were comparable across ReoV WT, ReoV-Q251*, ReoV-OVA, and ReoV-S21P2, indicating that σ1 modification does not impair viral fitness **(Figure 1F)**. Engineered viruses also show comparable or slightly higher lytic capabilities on L929 producer cells at 96 hpi, with ReoV-OVA and ReoV-S21P2 forming significantly larger plaques than ReoV WT and ReoV-Q251*(**Figure 1G, H**), suggesting an equal or potentially improved replication of the recombinant viruses. In summary, we established an optimized reverse genetics system for ReoV T3D variants displaying full antigens (SARS-CoV-2 RBD,) or immunogenic T cell epitopes (S21P2, OVA, $OVA^{323-339}$, Adpgk, Rpl18) successfully rescuing replication-competent recombinants with WT-comparable fitness. Finally, confirmed the safety profile of these recombinants by administering nine oral doses (1×10^9 $TCID_{50}$/dose) of either a vehicle control, ReoV WT, or ReoV-OVA to naïve C57BL/6 mice at the indicated time points, monitoring body mass daily before euthanasia, blood collection, and histochemical gut analysis (**Figure S1E**). No significant body mass loss was observed, and Hematoxylin and Eosin (H&E) staining revealed no intestinal villus atrophy or colon shortening, again highlighting the safety of this platform (**Figure S1F, H, I**). Lastly, detection and titration of neutralizing antibodies in the blood shows that repeated oral dosing (pink, 3-3-3, see **Figure S1E**) leads to significantly higher neutralizing antibody levels than a single intraperitoneal dose (dark red) or a single oral dose (red) (**Figure S1G**), emphasizing the validity of our hypothesis that oral administration of ReoV can induce a robust immune response.

Multi-route delivery of engineered reovirus activates antigen-specific immune responses

After demonstrating viral fitness and showing the feasibility and safety of oral administration, we next assessed whether the introduced epitopes could be processed, presented on MHC-I, and elicit antigen-specific immune responses. L929 cells stably expressing MHC-I-H2Kb were pulsed with scrambled peptide (negative control), SIINFEKL peptide (positive

control), or infected with ReoV WT, ReoV-Q251*, or ReoV-OVA. Immunoblotting at 72 hpi confirmed expression of bulk ReoV proteins, truncated σ1 from ReoV-Q251*, and Myc/FLAG-tagged σ1-OVA from ReoV-OVA **(Figure 2A**). Flow cytometric analysis using an anti-MHC-I-OVA antibody confirmed SIINFEKL presentation on MHC-I in at least 6% of ReoV-OVA–infected cells (**Figure 2B, S2A Top**). To assess in vivo $CD8^+$ T cell responses, naïve C57BL/6 mice were vaccinated three times over two weeks (1×10^9 $TCID_{50}$/dose, IV) with vehicle, ReoV-Q251*, or ReoV-OVA. Splenocytes harvested a week post-final vaccination were analyzed by interferon-gamma (IFN-γ) ELISpot following SIINFEKL stimulation. Compared to vehicle- and ReoV-Q251*–treated controls, ReoV-OVA–vaccinated mice showed significantly higher IFN-γ–secreting lymphocyte counts, confirming antigen-specific $CD8^+$ T cell activation and expansion (**Figure 2C**).

Repeating the experiment from **Figure 2C** via oral gavage (1×10^9 $TCID_{50}$/dose), ReoV-OVA–vaccinated animals again showed significantly higher SIINFEKL-specific IFN-γ^+ lymphocyte counts compared to vehicle and ReoV-Q251* controls (**Figure 2D**). To confirm functional $CD8^+$ T cell activation, L929-H2Kb cells infected with ReoV WT, ReoV-Q251*, or ReoV-OVA were co-cultured with OT-I splenocytes for 24 h, followed by intracellular cytokine staining for tumour necrosis factor alpha (TNF-α) and IFN-γ. ReoV-OVA–infected cells markedly increased the frequency of activated TNF-α^+IFN-γ^-, TNF-α^-IFN-γ^+, and double-positive $CD8^+$ T cells, while Mock, ReoV WT, and ReoV-Q251* groups showed no appreciable cytokine response (**Figure 2E, S2A, Bottom**). In addition to ReoV-OVA, to determine whether the engineered recombinant reovirus displaying the SARS-CoV-2 RBD induces a protective immune response, a dot-ELISA assay was performed, and viral samples were immobilized on a membrane and probed with specific antibodies to assess recognition of the inserted antigen **(Figure 2F, Top)**. SARS-CoV-2 neutralizing antibody produced a strong positive signal exclusively in the ReoV-RBD group, whereas Mock, ReoV WT, and ReoV-Q251* samples showed no detectable reactivity. As positive control, detection with an anti-reovirus antibody (α-ReoV) generated signals in all reovirus-containing groups, including ReoV WT, ReoV-Q251*, and ReoV-RBD, while the Mock control remained negative **(Figure 2F, Bottom)**. To evaluate vaccine efficacy of the ReoV-S21P2 platform, mice were immunized on days 0, 7, and 14 via either IP or PO routes, with serum and mucosal samples collected on day 21 (**Figure 2G, H**). IP administration (1×10^7 $TCID_{50}$/dose) elicited robust systemic IgG responses against Wuhan S and Fusion S proteins **(Figure 2G)**, while PO immunization induced significant mucosal IgA titers from intestinal washes reactive against both Spike variants **(Figure 2H)**. Finally, we were able to show that serum from vaccinated mice contained sufficient levels of neutralizing antibodies against SARS-CoV-2 Spike protein to markedly (**Figure S2D, E**) reduce infection of cells transduced to express the SARS-CoV-2 receptor hACE2 (**Figure S2C**) by a VSV pseudotyped with SARS-CoV-2 Spike protein (**Figure S2B**).

Prophylactic immunization with ReoV-OVA delays tumour onset and metastasis through antigen-specific immunity

Having confirmed that both IV and PO immunization with ReoV-OVA generated antigen-specific cytotoxic $CD8^+$ T cells, we evaluated the prophylactic potential of our vaccine platform against tumour challenges. We decided to use the B16F10 murine melanoma [22]. First, we

generated a B16F10 clone stably expressing full-length OVA via lentiviral transduction, confirming OVA expression by immunoblotting and SIINFEKL/MHC-I presentation by flow cytometry (**Figure 3A**). Then, to assess antigen-dependent therapeutic efficacy, mice were vaccinated with three weekly IP doses of either vehicle control, ReoV WT or ReoV-OVA (1×10^9 $TCID_{50}$/dose) followed by bilateral subcutaneous implantation of B16F10 (left flank) and B16F10-OVA (right flank) cells (1×10^6 tumour cells) (**Figure 3B)**. ReoV-OVA selectively suppressed the growth of B16F10-OVA tumour growth, whereas contralateral B16F10 tumours lacking OVA expression continued to progress. In contrast, ReoV WT failed to differentially control tumour growth at either flank, indicating a lack of antigen-specific therapeutic benefit. Notably, this effect was not attributed to direct viral oncolysis, as no viral proteins were detected in tumour lysates (**Figure S3A**).

Building on our previous finding that oral reovirus immunization elicits epitope-specific $CD8^+$ T cell responses **(Figure 2)**, we assessed its capacity to induce systemic antitumour immunity. Mice received three prophylactic PO doses of vehicle, ReoV WT, or ReoV-OVA (1×10^9 $TCID_{50}$/dose) prior to IV B16F10-OVA challenge to establish lung metastasis **(Figure 3C)**. At day 42, ReoV-OVA treatment profoundly restricted metastatic progression, yielding a mean tumour surface area of 29.93% versus 79.25% and 74.26% in vehicle and ReoV WT controls, respectively, as confirmed by gross inspection and H&E histology **(Figures 3D, F, S3B)**. This reduction in pulmonary burden translated into a significant survival advantage: while all control mice reached euthanasia criteria by day 28, ReoV-OVA–treated mice maintained significantly higher survival throughout the observation period **(Figure 3G)**. Collectively, these data demonstrate that engineered reovirus delivered orally primes a durable, systemic antitumour immune response capable of preventing and delaying tumour progression.

Virus replication is necessary for ReoV-OVA mediated cancer protection and is not affected by pre-exposure to virus.

Having established that the engineered ReoV-OVA platform elicits robust antigen-specific immunity and durable cancer control in multiple models (**Figures 2 and 3)**, we next sought to define the mechanistic requirements underlying this therapeutic effect. In particular, we asked whether viral replication is necessary for the observed antitumour efficacy, or whether non-replicative viral particles and therefore antigen delivery as protein alone is sufficient to promote immune-mediated tumour control. To test this, we infected BHK-21 cells with either vehicle, UV-inactivated ReoV-OVA, or untreated, replication-competent ReoV-OVA. Infection with replication-competent virus induced pronounced cytopathic effect (CPE) and extensive cell death, whereas UV-inactivated virus and vehicle controls showed no detectable cytotoxicity, demonstrating that UV irradiation successfully inactivated ReoV in this setting. In addition, we determined virus titers of the vehicle control, the inactivated preparation, and the parental, untreated virus stock by $TCID_{50}$ and were unable to detect infectious particles in the vehicle control and the inactivated virus preparation. In contrast, the titer of the parental virus stock was measured at 1.6×10^9 $TCID_{50}$/mL. **(Figure 4A)**. Consistent with these findings, immunoblot analysis confirmed robust expression of reoviral proteins and the Myc and FLAG -tagged σ1-OVA proteins exclusively in cells exposed to active ReoV-OVA, while UV-inactivated virus failed to generate detectable signals for viral proteins or transgenes **(Figure 4B)**. To investigate if virus replication

is necessary for proper immune activation as demonstrated previously, we used the same inactivated ReoV-OVA preparation and parental virus stock, to treat mice according to the timeline depicted in **Figure 4C**. Mice were immunized three times as indicated with either vehicle control, untreated ReoV-OVA or UV-inactivated ReoV-OVA prior to IV injection of B16F10-OVA cells. Importantly, only replication-competent virus mediated significant antitumour protection *in vivo*, whereas UV-inactivated virus was indistinguishable from vehicle-treated controls, establishing viral replication as a prerequisite for therapeutic efficacy **(Figure 4D, E, S4A)**.

Pre-existing exposure is a recurring topic of debate in virus-based therapies. Given the high seroprevalence of reovirus in the human population [23], it is plausible that pre-existing humoral immunity may influence the efficacy of reovirus-based immunotherapeutic approaches [24]. Therefore, we investigated if prior exposure to reovirus influences the virus' capacity to function as an effective cancer vaccine. To test this, we inoculated mice orally with ReoV WT six times (1×10^9 $TCID_{50}$/dose) to induce pre-existing exposure as indicated. Then, mice were vaccinated by two injections of ReoV-OVA (1×10^9 $TCID_{50}$/dose) on days 26 and 33 (**Figure 4F)** to confer anti-cancer immunity. After 5 days, B16F10-OVA tumour cells were injected IV. 30 days post tumour implantation mice were sacrificed, and the percentage of tumour surface area of the lungs was determined. Observed anti-tumour protection in mice with pre-existing exposure was not significantly different from those naïve to ReoV WT. In line with previous observations, mice that did not receive the ReoV-OVA cancer vaccine had significantly higher pulmonary tumour burdens **(Figure 4G, H, S4B)**. These results demonstrate that active viral replication is required for antitumour protection, as UV-inactivated virus particles were insufficient to induce immunity. Furthermore, although pre-existing exposure may attenuate viral replication, it did not impair OVA-specific antitumour protection elicited by ReoV-OVA.

ReoV cancer interception is limited by antigen expression and synergizes with checkpoint inhibition.

To further assess antigen-specific cancer control, mice were immunized three times by IP injection (1×10^9 $TCID_{50}$/dose) prior to right-flank implantation of B16F10-OVA cells (1×10^6). ReoV-OVA markedly suppressed tumour growth and significantly prolonged survival compared to ReoV WT, though three of ten animals developed rapidly progressing tumours despite vaccination **(Figure 5A)**. To confirm durable immune memory, the seven mice surviving past day 40 were re-challenged contralaterally with MC38-OVA cells. All rechallenged mice failed to develop detectable tumours and maintained long-term survival, demonstrating lasting antigen-specific memory (**Figure 5B, C**). Flow cytometric analysis of TILs revealed that ReoV-OVA treatment increased $CD45^+$ cell infiltration in B16F10-OVA tumours compared to ReoV WT ($p = 0.0520$), a trend absent in OVA-negative B16F10 tumours ($p = 0.9873$). Additionally, ReoV-OVA significantly shifted intratumoural T-cell composition toward the $CD8^+$ cytotoxic phenotype in B16F10-OVA tumours ($p < 0.05$), with no equivalent shift in antigen-negative tumours **(Figure 5D, S5D)**.

To investigate potential immune evasion mechanisms following ReoV-OVA vaccination, mice were immunized with either vehicle, ReoV WT, or ReoV-OVA as in **Figure 5A,** then 5×10^4 cells were implanted (B16F10 or B16F10-OVA). Delayed B16F10-OVA tumours from ReoV-

OVA–immunized mice showed visibly reduced melanin expression (**Figure 5E**), significant loss of OVA expression by immunoblotting compared to controls, alongside improved overall survival, indicating antigen loss under vaccine-induced immune pressure **(Figure 5F-H, S5B, S5C)**. Given the previously observed increase in $CD8^+$ T-cell infiltration, we investigated the expression of programmed death-ligand 1 (PD-L1) within the tumour microenvironment. Western blot analysis of tumour lysates showed that both ReoV WT and ReoV-OVA treatment led to a modest induction of PD-L1 expression compared to vehicle-treated controls with no significant difference between viral groups (**Figure 5I**), suggesting that therapeutic efficacy is limited by the induction of adaptive immune resistance via the PD-1/PD-L1 axis. To test this, mice bearing B16F10-OVA tumours were treated with oral immunizations of ReoV WT or ReoV-OVA in combination with IP injections of αPD-1(**Figure 5J)**. While αPD-1 monotherapy and ReoV WT+αPD-1 provided negligible survival benefits over vehicle controls, ReoV-OVA monotherapy significantly extended survival ($p < 0.05$), and, importantly, the combination of ReoV-OVA and αPD-1 resulted in a synergistic effect, profoundly extending the survival of tumour-bearing mice compared to treatment with ReoV-OVA alone ($p < 0.001$; **Figure 5J, S5E**). These results indicate that the delivery of tumour-specific antigens via ReoV sensitizes otherwise resistant B16F10 tumours to immune checkpoint blockade.

Discussion

A central challenge in cancer immunotherapy is the effective delivery of tumour antigens in a way that promotes robust, durable, and desired immune responses. Current vaccine, while effective in their respective ways, often are limited to intramuscular delivery. This is particularly problematic for preventing pathogens infecting and tumours originating from mucosal tissues, where systemic and mucosal immunities are both required for the best effect. In this study, we developed a ReoV-based vaccine platform that leverages its natural enteric tropism, resistance to acidic conditions, and clinically proved safety profile **(Figure 6)**. Our engineered attenuated ReoV constructs, capable of displaying a broad spectrum of antigens in the outer capsid protein σ1, successfully induced considerable systemic antibodies, including mucosal IgA, and antigen-specific $CD8^+$ T cell responses following oral, intravenous, and intraperitoneal delivery. Notably, oral vaccination prevented tumour onset and progression in multiple preclinical models of colorectal cancer (CRC), one of the most commonly occurring malignancy in the GI-tract. These findings establish proof-of-principle for an oral vaccine platform with broad implications for preventing infectious diseases and perhaps even modulating immune responses against cancer.

Several efforts have been made in the past to engineer ReoV as an expression vehicle. His_6 tag was first appended to the σ1 C-terminus using a helper-virus system, demonstrating feasibility of minor surface changes. With the development of plasmid-based reverse genetics, Brochu-Lafontaine et al. [25] showed that only short inserts (~40 nucleotides) were tolerated at the C-terminus of σ1, while Demidenko et al. successfully expressed multiple exogenous peptides from internal genome segments using 2A elements, confirming short-term genetic stability [26]. The insertion of a fluorescent protein (iLOV) into the σ1 region of a JAM-A-independent mutant (Jin) further validated the possibility of engineering replication-competent ReoV variants with altered surface structures. Boehme et al. extended this by displaying short HIV-1 gp41 epitopes in the α-helical domains of σ1, though this system did not elicit immune responses in preclinical models [27]. More recently, Kemp et al. engineered a *Jin-3* ReoV mutant to express GM-CSF from *S1* by

incorporating a P2A sequence after nucleotide position 768 [28]. Although the recombinant ReoV expressing GM-CSF enhanced dendritic cell recruitment and T cell priming in tumours, this system showed reduced rescue rate and genome instability [28]. While promising, these systems accumulate deleterious mutations over time, making continuous passage and maintenance of the recombinant virus difficult, which dramatically limited their usage clinically.

The modified ReoV vaccine platform contains an exchangeable antigen insertion and display site at amino acid position 250 in σ1. One distinct difference is that the design not only replaces the dispensable endogenous JAM-A binding domain with the antigen to-be-delivered but physically anchors it at the viral capsid for antigen stability and display. This design strategy was inspired by our previously reported RP116 variant with a truncated σ1. The long fibrous tail of σ1 projects the antigen away from the capsid, thus it provides sufficient spatial freedom for the proper folding and orientation of complex conformational epitopes while minimizing hindrance during particle assembly and infectivity [17, 29-31]. To further enhance the integrity of recombinant σ1 for oral delivery, we also incorporated a T249I mutation near its previously reported proteolytic cleavage site [32]. By presenting target antigenic peptide on the outer surface of reovirus, we effectively mimic authentic viral structures and epitopes, thereby facilitating B cell receptor crosslinking and antigen uptake for T cell priming [33]. Using this strategy, we were able to continuously replicate recombinant ReoV without deleterious mutations which permitted up-scaling of production. Importantly, we demonstrate that JAM-A-less ReoV is more resistant to neutralization from repetitive exposures that lead to reduced vaccination efficacy, which is commonly seen in adenovirus-based vaccines, effectively resolving the long-standing challenge of serum neutralization in virus-based vectors [17]. However, similar to other approaches, due to its proteinous capsids, larger transgenes may still be difficult to be incorporated into the viral genome. While *S1*-modified ReoV is excellent at displaying tandem repeats of linear B- and T-cell epitopes, large conformational epitopes that require a complex tertiary structure may lose their native form resulting in reduced efficacy or replication rate. However, this may be resolved by introducing other beneficial mutations that have been shown to increase viral fitness [34, 35].

The oral delivery of reovirus vaccine offers a distinct immunological advantage against respiratory pathogens and malignancies that arises within the intestinal mucosa, such as CRC. Unlike conventional parenteral vaccination approaches that predominantly induce systemic IgG responses and circulating effector T cells, oral reovirus vaccination directly engages GALT, thereby eliciting robust antigen-specific IgA mucosal immunity [3, 36, 37]. In our preclinical models, oral delivery of oncolytic wildtype reovirus led to robust infiltration of $CD8^+$ T cells into tumours and significant suppression of tumour growth and metastasis. Importantly, when combined with immune checkpoint inhibitors, oral reovirus vaccination resulted in complete tumour regression and generated protective memory responses that prevented tumour re-challenge, highlighting its capacity to induce durable antitumour immunity [14]. Moreover, the oncolytic properties of reovirus enable tumour-restricted replication and immunogenic cell death, effectively helping antigen spread within the host [38]. The intrinsic adjuvanticity can also be further harnessed in personalized immunotherapy by incorporating defined tumour neoantigens or minimal T cell epitopes into the viral capsid, enabling selective amplification of antigen-specific responses in the mucosa. As a needle-free vaccine, an oral reovirus vaccines carrying personalized CRC epitopes, can be easily self-administered as a prophylactic for individuals carrying germline susceptibility mutations, including Lynch syndrome, familial adenomatous polyposis, and other

hereditary CRC syndromes [39-41]. Supervised oral vaccination may also help keep raising waning immunity to prevent future infections and tumour recurrence with minimal clinical resources. Importantly, the natural stability of reovirus may reduce the transportation cost while increase dissemination in resource-limited settings or low-income nations. Thus, the innate acid resistance and gut tropism of reovirus holds great potential to overcome the long-standing obstacles faced by oral vaccines [6, 42].

Collectively, our findings establish ReoV as a versatile, live-attenuated vaccine platform capable of multi-route administration, particularly for oral delivery. Its ability to present tumour or pathogen-derived antigens on the capsid surface, induce coordinated mucosal and systemic immunity, and accommodate genetic modifications without compromising stability makes it ideally suited for next-generation vaccine development. By integrating the immunostimulatory potential of oncolytic virotherapy with precise antigen targeting, ReoV-based vectors offer a promising strategy for both infection control and cancer immunotherapy, especially at mucosal sites where conventional vaccines often fall short.

Materials and Methods

Mice

Six to eight-week-old female C57BL/6 mice were purchased from Charles River Laboratories, Wilmington, MA, USA. All *in vivo* experiments were conducted in faculty of medicine animal care facility at the university of Ottawa under the protocol CHEOe-4109. Animal care and experimental procedures were conducted in compliance with the ethical guidelines of the Canadian Council on Animal Care and the Animals for Research Act.

Six-week-old female C57BL/6 and BALB/c mice were purchased from NARA-Biotech (Seoul, South Korea) and ORIENT BIO Inc. (Seoul, South Korea), respectively for ELISPOT assay only. Mice were housed in an animal care facility at Virocure Inc. (Seoul, South Korea). All animal experiments were approved by the Institutional Animal Care and Use Committee (#VRC-2001) of Virocure Inc. and were carried out using approved protocols.

Cell Lines

In this study various cell lines, including L929, Vero, BHKT7, BHK21, murine melanoma cell lines (B16F10 and B16F10-OVA), L929-H2Kb, and murine colorectal cell lines (MC38 and MC38-OVA) were used. All cell lines were cultured Dulbecco's Modified Eagle Medium (DMEM) and maintained in 10% fetal bovine serum (FBS) and 1% penicillin/streptomycin in 37 °C in a 5% CO_2 incubator and they were routinely screened for mycoplasma contamination using Hoechst staining (NucBlue Live ReadyProbes Reagent, Invitrogen, Cat # R37605) and PCR (Diamed, Mississauga, Ontario; Cat # ABMG238) and were used within 5–15 passages following thawing. Of note, 2 µg/mL of puromycin was also added to those L929-H2Kb, B16F10-OVA and MC38-OVA transduced cells.

Animal Models and Treatment

Syngeneic Mouse Model

All tumour cells for implantation IV or SC were washed twice with PBS, counted using a Countess Automated Cell Counter, (Invitrogen, #10389053), then resuspended in 100 µL of PBS and kept on ice until the time of injection. In this model, the mice were then anesthetized by inhaled isoflurane and cells were injected subcutaneously. Tumours progression and development was regularly measured every other day using a digital caliper. Tumour volume was calculated using the following formula: $Tumor\ volume = \frac{(Length \times width^2)}{2}$, and width is representative of the smallest dimension of the tumour. Mice were euthanized according to the institutional guidelines review board for animal care. In addition, mice with any unwellness sign were also euthanized.

Metastasis Model

In this model, a week after the last immunization, 5×10^5 B16F10-OVA cells were injected IV using the tail vein. Mice were then euthanized three weeks after tumour cell injection, and the percentage of the lungs covered with tumour nodules were calculated using ImageJ software. However, in mouse metastasis survival model, pre-existing immunity model, and UV-inactivation model, 2.5×10^5 B16F10-OVA tumour cells were injected. Of note, mice were monitored daily for the signs of respiratory distress and any substantial impediment of physical activities resulted in mice euthanasia.

Combination Therapy Model

B16F10-OVA (1×10^5 cells in 100 µL of PBS) murine melanoma cells were injected subcutaneously under anesthesia. Once tumours reached palpable size, mice were randomly categorized into different groups and five rounds of oral immunization conducted on days 0, 2, 4, 6, and 8 as indicated in the respective figure. In parallel, mice were treated with 200 µg of α-PD1 (BioXCell, #BE0146) by IP injections on days 4, 6, 8, 11, and 14. Mice were euthanized once the tumour volume reached 2500 mm^3 in accordance with approved animal guidelines. Tumour volume was measured as described above.

Reovirus Rescue and Propagation

Reovirus was generated using a modified plasmid-based reverse genetic system established by Kobayashi *et al*. [21]. Briefly, confluent BHK-T7 cells, stably expressing T7 RNA polymerase (CVCL_A8V7, Cellosaurus), were seeded in a 60 mm dish and cultured until confluency (~ 1×10^6 cells/dish), cells were then co-transfected with a set of T7-promoter driven plasmids using TransIT-LT1 transfection reagent (Mirus, Cat. #MIR2300) according to the manufacturer's guidelines. This plasmid set includes pBacT7-S1 (3.8 µg) or equal amounts of recombinant plasmid encoding either S1-OVA, S1-Adpgk, or S1-Rpl18, together with plasmids encoding the other viral genome segments: pT7-L1 (Addgene, Cat. #33276) (2 µg), pT7-L2-M3 (Addgene, Cat. #33300) (2 µg), pT7-L3-M1 (Addgene, Cat. #33303) (2 µg), pT7-M2-S2-S3-S4 (Addgene, Cat. #300302) (2 µg), and helper plasmids: pCAG-FAST-p10 (Addgene, Cat. #89152) (20 ng), pCAG-D1R (Addgene, Cat. #89160) (2 µg), pCAG-D12L (Addgene, Cat. #89161) (2 µg), p-CAG-T7 (Addgene, Cat. #59926) (2 µg). Transfected cells were incubated in DMEM supplemented with 10% FBS at 37°C with 5% CO_2. After 72 hours or when cytopathic effect (CPE) became detectable, whichever came first, cell lysates and supernatants were collected. Cells were lysed by three freeze and thaw cycles to release intracellular virions. The resulting viral suspension was subsequently used to infect BHK-21 cells to amplify virus yield and to produce high-titer stocks, which were then purified by CsCl density gradient ultracentrifugation as described below in the Reovirus Purification section. In addition, UV-inactivated virus was generated by a UV-Cross linker. ReoV-OVA virus was irradiated with short-wave (254 nm) UV light on ice at a distance of 10 cm for 90 seconds at 180 mJ/cm^2 in a 6-well plate.

Reovirus titration

L929 cells (4×10^4 cells/well) were seeded in a 96-well plate and allowed to reach the 90% confluency. Serial 10-fold dilutions of the purified virus were prepared in DMEM containing 10% FBS and 100 µL of each dilution was added to the wells in quintuplicate. Following incubation at 37°C with 5% CO_2 for 72 hours, cells were fixed with 100 µL of 7.4% PFA added to 100 µL of medium in culture. After blocking with Triton X-100, viral antigens were detected by primary antibodies, including anti-T3D serum (rabbit, 1:1000 dilution) and anti-FLAG tag mAb (mouse, 1:1000 dilution, Sigma, #F1804-200). Primary antibodies were detected by fluorescent-labelled secondary antibodies. Wells were considered positive for virus infection by detection of cells foci on GFP channel. $TCID_{50}$/mL was calculated using the Reed–Muench method based on the proportion of antibody-spositive wells at each dilution.

Reovirus purification

Reovirus was propagated in BHK-21 cells grown in DMEM supplemented with 10% FBS and 1% penicillin–streptomycin (Cytiva, Cat #SV30010). Once CPE was observed, cells and supernatants

were harvested and subjected to three freeze and thaw cycles to release intracellular virions. Cell debris was removed by centrifugation at 1935 *g* at room temperature using Beckman bottles with the JLA-10500 rotor for 10 minutes. The supernatant was then centrifuged for 2 hours at 12096 *g* at 4°C using the same bottles and rotors to pellet the virus. The pellet was resuspended in DMEM and layered onto a cesium chloride gradient (FisherBio Tech, #BP210-500) (1.40 and 1.25 g/mL respectively,) and viral particles were concentrated by ultracentrifugation at 115460 *g* for 2 hours at 12°C. Then, the lower of two visible bands (containing complete virions) was extracted using a 20G needle and syringe, diluted up to 21 mL using PBS and layered onto a cesium chloride cushion (1.38 g/mL) in Beckman Ultraclear tubes (Sigma, #746487) and again concentrated by ultracentrifugation at 115460 *g* for 2 hours in 12°C. After this, the single band was extracted (see above) and loaded into a 20,000 MWCO Slide-A-Lyzer dialysis cassette (Life Technologies, Cat #66012) pre-soaked in PBS and dialysis was performed against 500 mL of PBS over night and continued the following day by exchanging the PBS every 2 hours for a total of three changes. The virus was then extracted from the cassette, aliquoted, and stored at -80 °C until further use.

Western blotting

Cells were harvested by scraping and lysed in RIPA buffer (Sigma, #R028750ML) containing protease inhibitors (Thermo Fisher Scientific, Cat. #87785) and protein concentrations were determined using Pierce Dilution-Free Rapid Gold BCA Protein assay kit (Life Technologies, CAT #A55861) according to the manufacturers' guidelines. Equal amounts of protein (20 µg) were separated on 10% stain-free SDS-PAGE (Bio-Rad, #1610183) and transferred on polyvinylidene fluoride (PVDF) membranes using semi-dry transfer (Bio-Rad, Cat. #10026938). Membranes were then blocked by incubating with Everyblot blocking buffer (Bio-Rad, Cat. #12010020), washed 3 times with Tris-Buffered-Saline-Tween (TBS-T), and then incubated overnight at 4°C with the following primary antibodies at the indicated dilutions: anti-T3D serum, rabbit (1:1000), anti Flag-tag (clone D6W5B) mAb, rabbit (1:1000, NEB, Cat. #14793S), anti Flag-tag mAb, mouse (1:1000, Sigma, Cat. #F1804-200ug), anti-Myc-Tag (clone 9B11) mAb, mouse (1:1000, Cell Signalling, Cat. #2276S), anti-Myc-Tag (clone 71D10) mAb, rabbit (1:1000, Cell Signalling, Cat. #2278S), and anti-Ovalbumin, rabbit (1:1000, Novus Biologicals, Cat. #NB600-922). After three times of washing with TBS-T, the membranes were then incubated with secondary antibodies for 1 h at room temperature, including IRdye 800CW goat anti-rabbit (1:5000, Licor, Cat. #92632211) and IRdye 680RD goat anti-mouse (1:5000, Licor, Cat. #92668070). All antibodies used for immunoblotting were diluted in TBS (Licor, Cat. #927-60001) according to the manufacturer's recommendations. Then, membranes were washed again three times with TBS-T and protein bands were visualized and quantified using a Licor Odyssey imaging system and signal intensities were normalized to β-actin (1:5000, Sigma, Cat. #A5441).

RT-qPCR

Total RNA was extracted using RNeasy Mini kit (Qiagen, Hilden, Germany), DNase-treated with TURBO DNA-*free*™ kit (Cat# Thermo Scientific) and reverse transcribed into cDNA using iScript Advanced cDNA Reverse Transcription kit (Bio-Rad, Cat. #1725037). Quantitative PCR of the synthesized cDNA was performed on a CFX96 Touch Real-Time PCR Detection System (Bio-Rad, Hercules, CA) using SsoAdvanced™ Universal SYBR® Green Supermix (Bio-Rad, Cat. #1725271). All primers were used at a concentration of 500 nM with their respective qPCR program (see Supplemental Table S1 for primer sequences). All qPCR assays were performed using the following program unless otherwise specified: 95 ℃ for 3 min followed by 45 cycles of

95 ℃ for 10 sec and 60 ℃ for 30 sec). Relative expression was determined using the comparative Ct method. All the primers have been listed in **supplementary Table 1**.

Tissue Processing

Tumours were dissociated using a Mouse Tumour Dissociation Kit in conjunction with a gentleMACS Octo Dissociator (both from Miltenyi Biotec, Cat. #130-096-730 and #130-096-427, respectively, CA. USA). Splenocytes were isolated by mechanically disrupting the tissue through a 70 µm strainer using a 3 mL syringe plunger, followed by erythrocyte lysis with ACK buffer (Gibco). Resulting cell suspensions were filtered and quantified. For flow cytometry, 2×10^6 cells were resuspended in 200 µL of FACS buffer (PBS containing 0.5% BSA) and transferred to round-bottom 96-well plates. Alternatively, for *in vitro* applications, tumour cells or splenocytes were resuspended in 100 µL of RPMI medium supplemented with 10% heat-inactivated FBS.

Flow cytometry

Single-cell suspensions were incubated with Zombie Green Fixable Viability Kit (1:1000; BioLegend) for 15 min at room temperature. To prevent non-specific binding, cells were blocked with anti-CD16/32 (1:100; BioLegend) in 0.5% BSA-PBS for 30 min at 4°C. Surface staining was performed using an antibody cocktail diluted in 0.5% BSA-PBS. Following staining, cells were fixed in 1% PFA. Then, Samples were acquired on a BD LSRFortessa™ (FACSDiva™ v9) at CHEO research institute. Data was analyzed via FlowJo v10.8, with dimensionality reduction performed using opt-SNE. Controls included unstained cells, fluorescence-minus-one (FMO) tubes, and UltraComp eBeads (Thermo Scientific) for compensation. All flow cytometry antibodies have been listed in **supplementary Table 2.**

Enzyme-linked immunospot (ELISPOT) assay

The strip plate, pre-coated with IFN-γ (Mabtech, Sweden, #3321-4AST-2) was washed four times with sterile PBS, then conditioned with RPMI 1640 medium (200 µL/well) for half an hour at room temperature. Splenocytes of immunized mice were collected and incubated in RPMI 1640 medium (1×10^6 cell/well, 200 µL/well) supplemented with 10% FBS and 1% penicillin–streptomycin in pre-coated strip plate. Then, cells were stimulated with 10 µg/mL of SIINFEKL peptide. IFN-γ secretion was visualized by incubation with biotin-conjugated anti-IFN-γ antibody (Mabtech, Sweden, #3321-4AST-2), followed by streptavidin-alkaline phosphatase (Mabtech, Sweden, #3321-4AST-2) and BCIP/NBT substrate (Mabtech, Sweden, #3321-4AST-2). Then, wells were air-dried and the number of spots were counted. Spot counts obtained from unstimulated or DMSO-treated control wells were considered background and subtracted from all corresponding experimental conditions within the same sample.

Immunofluorescence (IF) Staining

Vero cells were cultured in DMEM on sterile glass coverslips overnight at 37°C and 5% CO_2. Cells were then infected with either ReoV WT or ReoV-OVA using infected cells' supernatant. 48 hours post-infection (hpi) cells were fixed with 3.7% paraformaldehyde (PFA) and stained with anti-ReoV serum (1:1000, rabbit), anti-Myc-Tag (9B11) mouse mAb (1:200, Cell Signalling, Cat. #2276S), and anti-Flag-Tag mouse mAb (1:1000, Sigma, Cat. #F1804-200ug), respectively, for 1 hour. Primary antibodies were then detected after 45 minutes of incubation with anti-rabbit- Alexa Fluor 488 (Thermo Fisher Scientific, 1:200, Cat. #A-11017), and anti-mouse Alexa Fluor 594

(Thermo Fisher Scientific, 1:200, Cat. #A-11020). The coverslips were mounted Flourmount G with DAPI for nuclear counter stain and stored at 4°C. Microscopic images were taken with an Olympus confocal microscope with a 60X oil immersion objective.

Indirect ELISA for the evaluation of humoral responses

The same SARS-CoV-2 Wuhan S and the Fusion S conformation antigens that were administered for immunizations for used as coating antigens for serological assays. Antibody responses were evaluated as previously described in Maltseva et al. Wuhan S protein and the Fusion S were diluted in sterile 1X PBS (Wisent Bioproducts, 311-010-CL, St-Bruno, QC, Canada) to 4 µg/mL and coated onto 384-well Immuno plates (Thermo Fisher, #60372, Waltham, MA, USA) (10 µL/well) overnight at 4 °C. Plates were washed three times with 100 µL of PBS-T and blocked for 1 h with a blocking buffer (PBS-T + 3% non-fat milk powder, *w*/*v*) on a shaker at room temperature. Serum samples were diluted 1:25 following third immunization, and intestinal supernatant samples, concentrated from 0.5 mL using an Ambicon filter with a 10-k cutoff, were diluted 2-fold in dilution buffer (PBS-T + 1% non-fat milk powder, *w*/*v*). After blocking, plates were washed thrice with PBS-T and followed by addition of 10 µL of the respective diluted samples. The plates were incubated for 2 h on a shaker at room temperature, washed thrice with PBS-T followed by the addition of 10 µL of the respective secondary-HRP antibody at specified dilutions: 1:4000 secondary IgG Anti-Mouse, Human ads-HRP (Southern Biotech, 1030-05, Birmingham, AL, USA) and 1:1000 secondary Anti-Mouse IgA-HRP (Southern Biotech, 1040-05, Birmingham, AL, USA). Plates were incubated for 1 h on a shaker, washed thrice with PBS-T followed by the addition with 10 µL of the SuperSignal ELISA Pico Chemiluminescent Substrate (Thermo Scientific, 37069, Waltham, MA, USA). Luminescence intensity was measured with BIO-TEK Synergy Neo2 plate reader for 20 ms/well at a read height of 1.0 mm. Wells filled with dilution buffer in place of sample accounted for background luminescence and were subtracted from the sample values.

Serum neutralization assays

Neutralizing antibody responses against reovirus were analyzed using serum collected from mice 14 days post-infection. Serum samples were serially diluted 2-fold (final dilutions ranging from 1:10 to 1:10240) in DMEM in 96-well plates, with a total volume of 60 µL per well. An equal volume (60 µL) of reovirus suspension containing 6,000 $TCID_{50}$ was added to each well, and the virus–serum mixtures were incubated at 37°C for 1 hour to facilitate neutralization. Subsequently, 100 µL of serum/virus suspension was added on 4×10^5 of previously cultured L929 cells/well, and plates were incubated for 72 hours at 37°C. The CPE was monitored microscopically, and neutralization titers were calculated as the $\log_{10}$ of the reciprocal serum dilution that inhibited CPE in 50% of wells compared with virus-only controls. All assays were conducted independently at least twice to ensure reproducibility.

Statistical analysis

All experiments were performed independently at least three times ($n \geq 3$). The exact number of times each experiment was performed is indicated in the figure legends while the individual data points are displayed on the graphs. Data are shown as mean ± SD, which were subjected to unpaired two-tailed Student's t tests and analysis of variance followed by Tukey's or Bonferroni post hoc tests. A $p < 0.05$ was considered statistically significant. Correlation analysis was performed using Spearman's rank correlation test and the survival rate was determined by the

Kaplan-Meier method. Statistical significance was also calculated using the same program and was considered statistically significant when the p value was < 0.05.

Conflict of interest

K-H.S., Y-K. L. and W-J. L are affiliated with ViroCure Inc. T.A. and X.X. have a consulting and advisory role at ViroCure, CuroV Science and Genvira Biosciences. The other authors declared no conflict of interest related to this work.

Acknowledgements

This research was partially supported by the New Chongqing Talent Recruitment Program: Excellent Young Scientists Fund (CSTB2024YCJH-KYXM0085), a by a Natural Sciences and Engineering Research Council of Canada (NSERC) Discovery Grant (RGPPIN-2024-05595), Canadian Cancer Society Research Institute Challenge Grant (#707351), Cancer Research Society, Canadian Institute of Health Research (CIHR #525961), and BioCanRx funding (#CAT21).

Author contributions

T.A. and X.X. proposed and supervised the project. S.P., X.X., Y.L., K-H.S., N.S., E.W., S.T., M.M., K.M., C.R.G., A-D.Y., T.F., J.P., N.E., and H-D.H. performed the experiment. X.X., M-A.L., G.L., Y-K.L., H-D.H. K.H., J.W., J.C.B., W-J.L. S.T.B., and T.A. were involved in the conceptual design. S.P., X.X., N.T.M. and T.A. wrote the manuscript. S.P. and X.X. performed data analysis. S.P., X.X., and N.T.M. designed the figured and illustrations. All authors read and approved the final manuscript.

Data availability

The data supporting the findings of this study are available within the article and its Supplementary Information and can be made available for research purposes from the corresponding author upon reasonable request.

Supplementary information

Supplementary Figures
Supplementary Tables

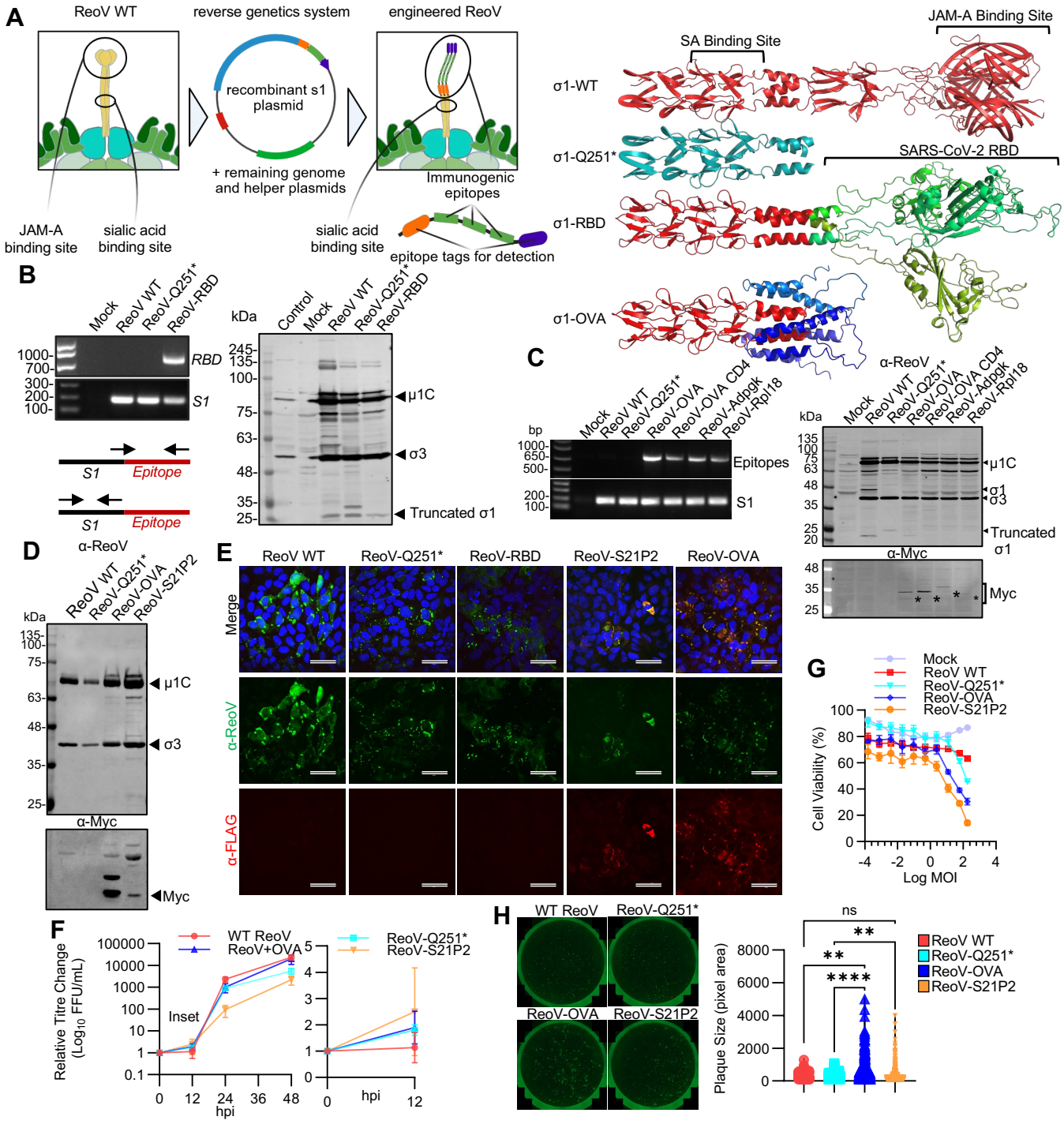
References

1. Becker, W. and W.K. Rathmell, *Vaccines in cancer treatment and prevention: the time is now.* J Clin Invest, 2025. **135**(13).
2. Morens, D.M. and A.S. Fauci, *Emerging Pandemic Diseases: How We Got to COVID-19.* Cell, 2020. **182**(5): p. 1077-1092.
3. Lavelle, E.C. and R.W. Ward, *Mucosal vaccines - fortifying the frontiers.* Nat Rev Immunol, 2022. **22**(4): p. 236-250.
4. Miquel-Clopés, A., et al., *Mucosal vaccines and technology.* Clin Exp Immunol, 2019. **196**(2): p. 205-214.
5. Liu, Y., et al., *Recent development of oral vaccines (Review).* Exp Ther Med, 2024. **27**(5): p. 223.
6. Kwong, K.W., et al., *Oral Vaccines: A Better Future of Immunization.* Vaccines (Basel), 2023. **11**(7).
7. Kunisawa, J., Y. Kurashima, and H. Kiyono, *Gut-associated lymphoid tissues for the development of oral vaccines.* Adv Drug Deliv Rev, 2012. **64**(6): p. 523-30.
8. Kim, H., et al., *Gastrointestinal Delivery of an mRNA Vaccine Using Immunostimulatory Polymeric Nanoparticles.* Aaps j, 2023. **25**(5): p. 81.
9. Kang, S.H., et al., *Oral Vaccine Delivery for Intestinal Immunity-Biological Basis, Barriers, Delivery System, and M Cell Targeting.* Polymers (Basel), 2018. **10**(9).
10. Müller, L., et al., *Past, Present and Future of Oncolytic Reovirus.* Cancers (Basel), 2020. **12**(11).
11. Boehme, K.W., C.M. Lai, and T.S. Dermody, *Mechanisms of reovirus bloodstream dissemination.* Adv Virus Res, 2013. **87**: p. 1-35.
12. Alain, T., et al., *Proteolytic disassembly is a critical determinant for reovirus oncolysis.* Mol Ther, 2007. **15**(8): p. 1512-21.
13. Alain, T., et al., *The oncolytic effect in vivo of reovirus on tumour cells that have survived reovirus cell killing in vitro.* Br J Cancer, 2006. **95**(8): p. 1020-7.
14. Lee, W.S., et al., *Oral reovirus reshapes the gut microbiome and enhances antitumor immunity in colon cancer.* Nat Commun, 2024. **15**(1): p. 9092.
15. Lin, Q.F., et al., *Reovirus genomic diversity confers plasticity for protease utility during adaptation to intracellular uncoating.* J Virol, 2023. **97**(10): p. e0082823.
16. Sharifi, N., et al., *Reovirus oncolysis and the next frontiers for this unique oncoviral immunotherapy.* Semin Immunol, 2025. **80**: p. 101995.
17. Song, K.H., et al., *The reovirus variant RP116 is oncolytic in immunocompetent models and generates reduced neutralizing antibodies to Type 3 Dearing.* Mol Ther Oncol, 2024. **32**(3): p. 200846.
18. Kim, M., et al., *Attenuated reovirus displays oncolysis with reduced host toxicity.* Br J Cancer, 2011. **104**(2): p. 290-9.
19. Hos, B.J., et al., *Identification of a neo-epitope dominating endogenous CD8 T cell responses to MC-38 colorectal cancer.* Oncoimmunology, 2019. **9**(1): p. 1673125.
20. Zhou, S., et al., *Identification of Enhanced Vaccine Mimotopes for the p15E Murine Cancer Antigen.* Cancer Res Commun, 2024. **4**(4): p. 958-969.
21. Kobayashi, T., et al., *A plasmid-based reverse genetics system for animal double-stranded RNA viruses.* Cell Host Microbe, 2007. **1**(2): p. 147-57.
22. Fidler, I.J., *Biological behavior of malignant melanoma cells correlated to their survival in vivo.* Cancer Res, 1975. **35**(1): p. 218-24.

23. Groeneveldt, C., et al., *Neutralizing Antibodies Impair the Oncolytic Efficacy of Reovirus but Permit Effective Combination with T cell-Based Immunotherapies.* Cancer Immunol Res, 2024. **12**(3): p. 334-349.
24. Berkeley, R.A., et al., *Antibody-Neutralized Reovirus Is Effective in Oncolytic Virotherapy.* Cancer Immunol Res, 2018. **6**(10): p. 1161-1173.
25. Brochu-Lafontaine, V. and G. Lemay, *Addition of exogenous polypeptides on the mammalian reovirus outer capsid using reverse genetics.* J Virol Methods, 2012. **179**(2): p. 342-50.
26. Demidenko, A.A., et al., *Engineering recombinant reoviruses with tandem repeats and a tetravirus 2A-like element for exogenous polypeptide expression.* Proc Natl Acad Sci U S A, 2013. **110**(20): p. E1867-76.
27. Boehme, K.W., et al., *Engineering Recombinant Reoviruses To Display gp41 Membrane-Proximal External-Region Epitopes from HIV-1.* mSphere, 2016. **1**(3).
28. Kemp, V., et al., *Arming oncolytic reovirus with GM-CSF gene to enhance immunity.* Cancer Gene Ther, 2019. **26**(9-10): p. 268-281.
29. Koehler, M., et al., *Reovirus directly engages integrin to recruit clathrin for entry into host cells.* Nat Commun, 2021. **12**(1): p. 2149.
30. Garcia, M.L. and P. Danthi, *The Reovirus σ1 Attachment Protein Influences the Stability of Its Entry Intermediate.* J Virol, 2023. **97**(5): p. e0058523.
31. Dietrich, M.H., et al., *Structural and Functional Features of the Reovirus σ1 Tail.* J Virol, 2018. **92**(14).
32. Fernandes, J.P., et al., *Breast Tumor-Associated Metalloproteases Restrict Reovirus Oncolysis by Cleaving the σ1 Cell Attachment Protein and Can Be Overcome by Mutation of σ1.* J Virol, 2019. **93**(22).
33. Chappell, J.D., et al., *Crystal structure of reovirus attachment protein sigma1 reveals evolutionary relationship to adenovirus fiber.* Embo j, 2002. **21**(1-2): p. 1-11.
34. Mohamed, A., R.N. Johnston, and M. Shmulevitz, *Potential for Improving Potency and Specificity of Reovirus Oncolysis with Next-Generation Reovirus Variants.* Viruses, 2015. **7**(12): p. 6251-78.
35. Kemp, V., R.C. Hoeben, and D.J. van den Wollenberg, *Exploring Reovirus Plasticity for Improving Its Use as Oncolytic Virus.* Viruses, 2015. **8**(1).
36. Marking, U., et al., *Impact of systemic SARS-CoV-2 vaccination on mucosal IgA responses to subsequent breakthrough infection.* EBioMedicine, 2025. **120**: p. 105912.
37. Neutra, M.R. and P.A. Kozlowski, *Mucosal vaccines: the promise and the challenge.* Nat Rev Immunol, 2006. **6**(2): p. 148-58.
38. Palanivelu, L., C.H. Liu, and L.T. Lin, *Immunogenic cell death: The cornerstone of oncolytic viro-immunotherapy.* Front Immunol, 2022. **13**: p. 1038226.
39. Sei, S., et al., *Lynch syndrome cancer vaccines: A roadmap for the development of precision immunoprevention strategies.* Front Oncol, 2023. **13**: p. 1147590.
40. Esplin, E.D., et al., *Multiomic analysis of familial adenomatous polyposis reveals molecular pathways associated with early tumorigenesis.* Nat Cancer, 2024. **5**(11): p. 1737-1753.
41. D'Alise, A.M., et al., *Nous-209 neoantigen vaccine for cancer prevention in Lynch syndrome carriers: a phase 1b/2 trial.* Nat Med, 2026. **32**(3): p. 1002-1011.

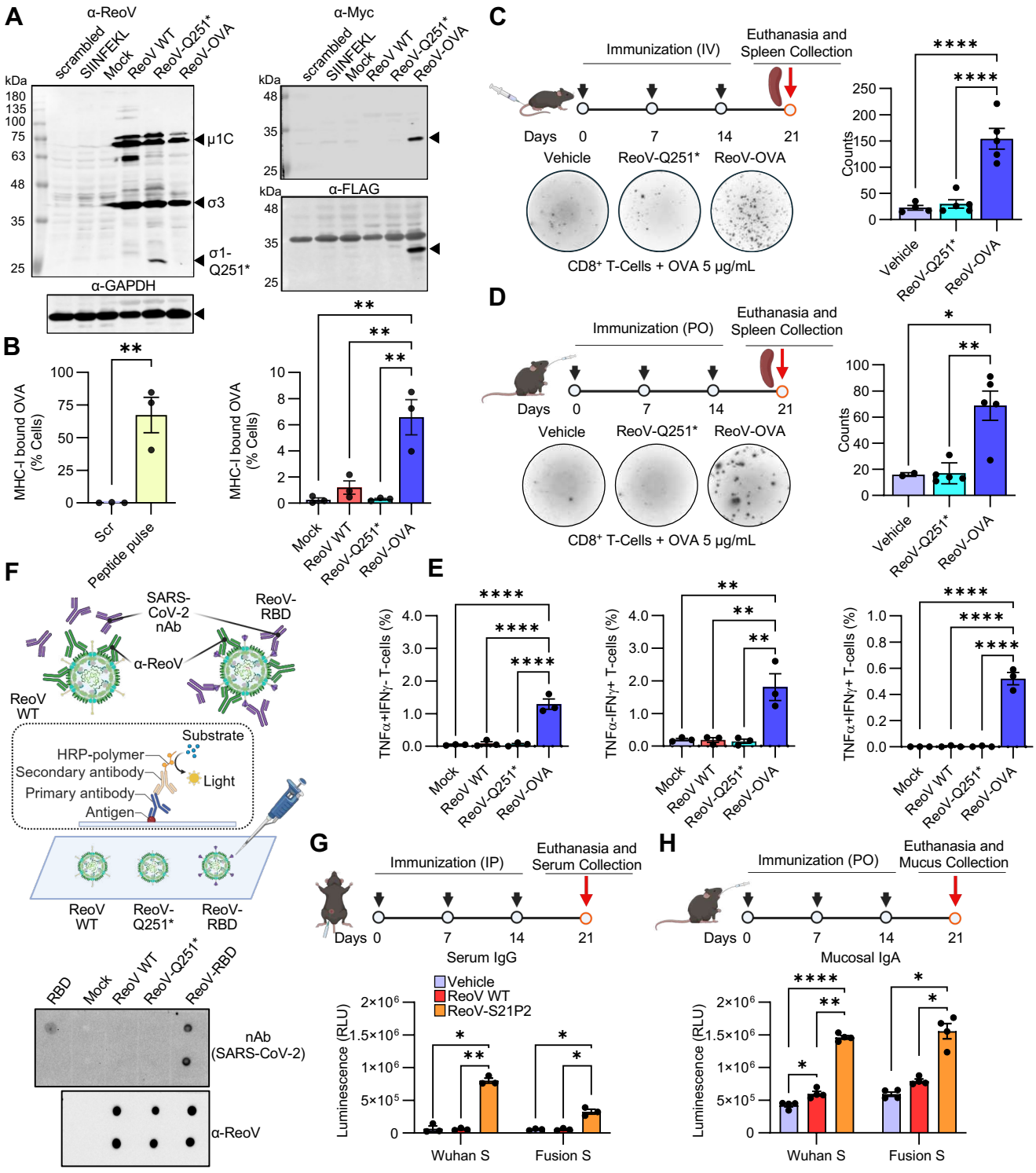
42. Glorani, G., et al., *An Unusual Aspartic Acid Cluster in the Reovirus Attachment Fiber σ1 Mediates Stability at Low pH and Preserves Trimeric Organization.* J Virol, 2022. **96**(8): p. e0033122.

Figure 1



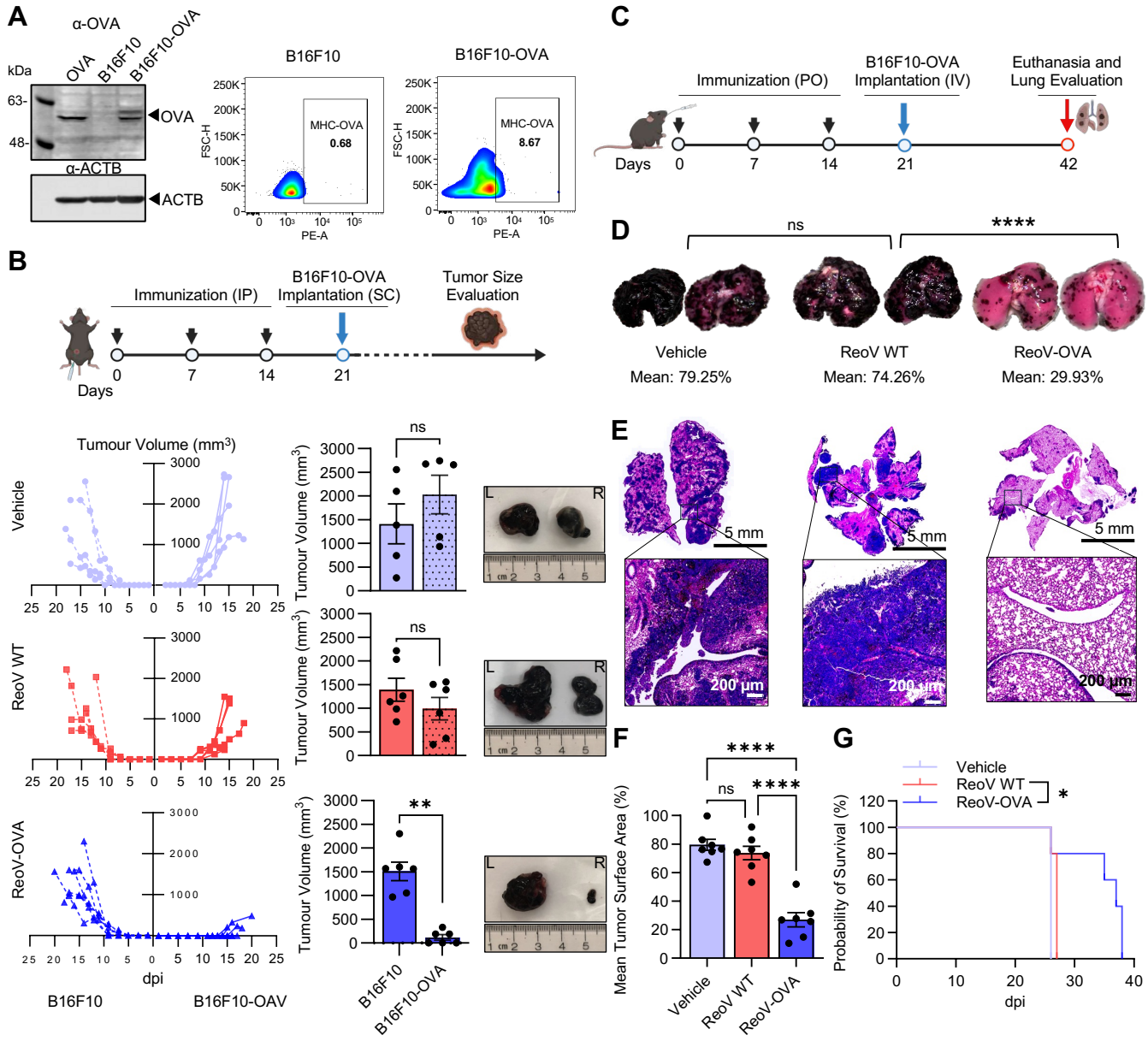
Reovirus can be engineered with immunogenic epitopes while maintaining replication. (**A**) Left: ReoV WT can be engineered using a reverse genetics system to encode epitopes in the *S1* gene which are displayed on the virion, replacing the JAM-A binding domain while leaving the sialic acid binding domain intact. Larger antigens (RBD of SARS-CoV-2) can also be incorporated. Right: Tertiary structures (σ1-WT, σ1-Q251*), AlphaFold prediction (σ1-RBD), and a schematic of the linear constructs. (**B-D**) ReoV WT and variants containing either a truncated σ1 protein (Q251*), the RBD of SARS-CoV-2, the MHC-I OVA epitope (OVA), the MHC-II OVA epitope (OVA CD4), MC38 neoepitopes (Adpgk and Rpl18), or an epitope from RBD (S21P2) can be rescued as confirmed by immunoblotting against bulk ReoV proteins (top) and Myc-tagged σ1 recombinants (bottom). Recombinant gene segments can be detected PCR. Primer design given below. (**E**) IF of Vero cells infected with ReoV WT, ReoV-Q251*, ReoV-RBD, ReoV-S21P2, or ReoV-OVA as indicated demonstrates colocalization of viral proteins. Cells were stained for ReoV (green; α-ReoV), Flag-tag (red; α-Flag), and DAPI (blue). Scale bar = 50 μm. Engineered ReoVs show growth kinetics(**F**) and lytic capabilities (**G**) comparable to the WT. Virus growth curve at an MOI of 10 for L929 cells during 48 hpi (left), and during the first 12 hpi (right). Cell viability (Alamar blue) assessed 96 hpi with ReoV WT, ReoV-Q251*, ReoV-OVA, or ReoV-S21P2 at the indicated MOI. (**H**) ReoV-OVA forms significantly larger plaques (48 hpi) than ReoV WT and ReoV-Q251*, while ReoV-S21P2 plaques are significantly larger than ReoV-Q251*, but not ReoV WT. All data points represent mean ± SEM. hpi = hours post infection, IF = immunofluorescence microscopy, IP = intraperitoneal, MOI = multiplicity of infection, PO = per os, orally, RBD = receptor binding domain, ReoV = Reovirus, WT = wildtype.

Figure 2



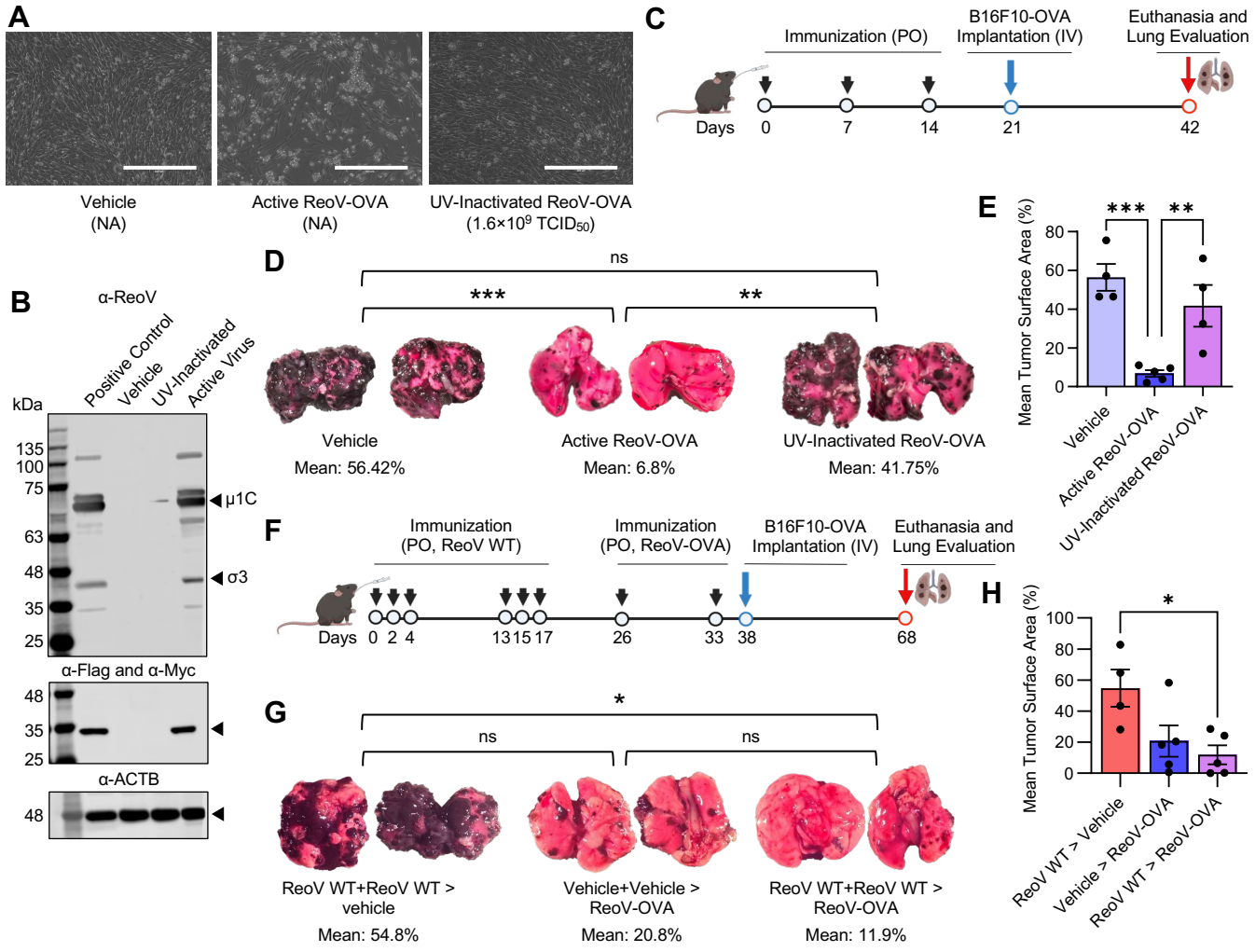
Immunization with recombinant ReoVs induces an epitope-specific immune response. (**A**) Representative immunoblots of cell lysates from MHC I (H-2Kb)-transduced L929 cells following infection with different ReoV variants or peptide controls. Antibodies against the flanking tags (Myc and FLAG) allow for detection of the OVA transgene (**B**) Flow cytometric analysis of MHC-I-bound SIINFEKL peptide on H-2Kb transduced L929 cells. Cells pulsed with SIINFEKL peptide compared to scrambled peptide (left). Percentage of MHC-I-bound SIINFEKL peptide on H-2Kb transduced L929 cells following infection with ReoV WT, ReoV-Q251*, or ReoV-OVA (n = 3). (**C**) IV and (**D**) PO immunization with ReoV induces an OVA-specific CD8⁺ T cell response. Mice were immunized with vehicle, ReoV-Q251*, or ReoV-OVA (1×10^9 $TCID_{50}$/dose) in a prime-boost-boost regimen and splenocytes were analyzed using ELISpot assay. (n = 5). (**E**) Quantification of activated CD8⁺ cells by TNF-α and IFN-ɣ using OT-I mice splenocytes after co-culture with different variants of reovirus, including ReoV WT, ReoV-Q251*, and ReoV-OVA (n = 3). (**F**) Dot-ELISA (Top: schematic) shows engineered ReoV-RBD can be recognized by an nAb against SARS-CoV-2 (bottom). (**G**) IP immunization with ReoV-RBD, but not with vehicle, or ReoV-WT (1×10^7 $TCID_{50}$/dose, n = 3) leads to a significant level of neutralizing serum IgG against both SARS-CoV-2 Spike protein (Wuhan strain and in fusion conformation). (**H**) PO immunization with ReoV-RBD, but not with vehicle, or ReoV-WT (1×10^7 $TCID_{50}$/dose, n = 3 in all groups) leads to a significant level of neutralizing mucosal IgA obtained from intestinal washes against both SARS-CoV-2 Spike protein (Wuhan strain and in fusion conformation). All data points represent mean ± SD. P-value calculated by one-way ANOVA. *p < 0.05, **p < 0.01 and ****p < 0.0001. IP = intraperitoneal, nAb = neutralizing antibody, PO = per os, orally, RBD = receptor binding domain, ReoV = Reovirus, WT = wildtype.

Figure 3



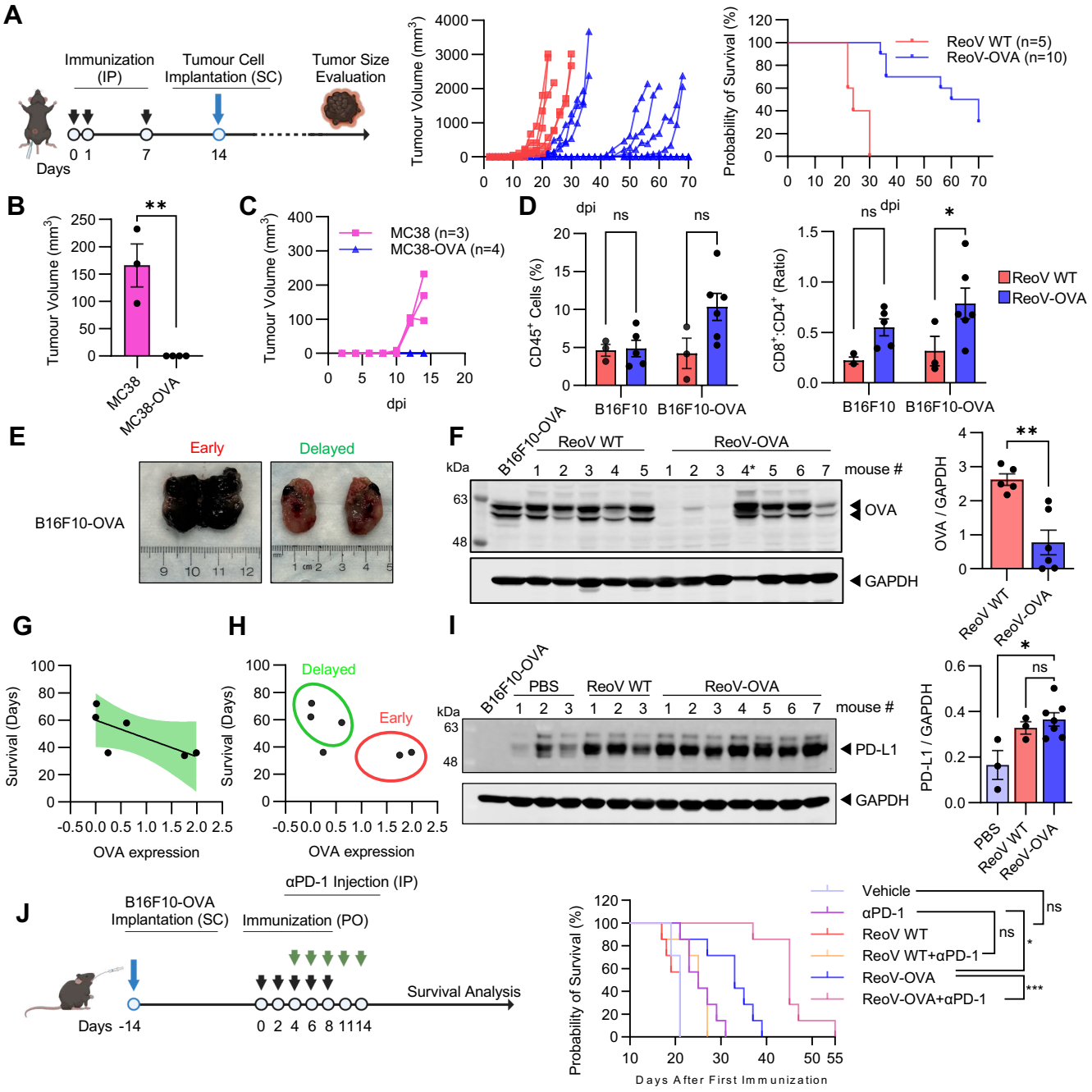
Immunization with ReoV-OVA delays tumour onset and metastasis. (**A**) Immunoblotting against Ovalbumin (left) and flow cytometric analysis (right) of MHC-I bound SIINFEKEL peptide shows expression and presentation of the targeted epitope on B16F10 cells after lentiviral transduction. (**B**) Immunization schedule. C57BL/6 mice were immunized with ReoV WT or ReoV-OVA (1×10^9 $TCID_{50}$/dose) through IP injection on a prime-boost-boost plan. On day 21, 3×10^6 of B16F10 and B16F10-OVA cells were injected SC into the left and right flank of the mice, respectively. (*n* = 6 mice per group). Tumour volume over time for each flank shows delayed tumour progression in immunized mice. (**C**) Schedule for metastasis model immunization. On days 0, 7, and 14, mice were immunized PO with either vehicle, or 1×10^9 $TCID_{50}$/dose of ReoV WT or ReoV-OVA (*n* = 7 in each group). On the indicated day, 5×10^5 B16F10-OVA cells were implanted IV through the tail vein. On day 42, mice were euthanized and the lungs collected. (**D**) Representative images of two lungs from each group, showing a reduced tumour burden in animals immunized with ReoV-OVA as indicated by a significant reduction of melanin positive tumour nodules. (**E**) Representative histological section (H&E staining) of the tissue showing reduced infiltration with melanin positive cells in animals immunized with ReoV-OVA. (**F**) Quantitative assessment of the tumor burden calculated as the mean percentage of tumour surface area across lungs' lobes. (**G**) Mice overall survival shows a significant survival benefit for animals treated with ReoV-OVA. All Data points represent mean ± SD. For analysis of survival data, *P*-values were calculated by the Kaplan–Meier method followed by log-rank/mantel-Cox test. ns; non-significant, *p < 0.05, **p < 0.01 and ****p < 0.0001. IP = intraperitoneal, MOI = multiplicity of infection, PO = per os, orally, ReoV = Reovirus, SC = subcutaneous, WT = wildtype.

Figure 4



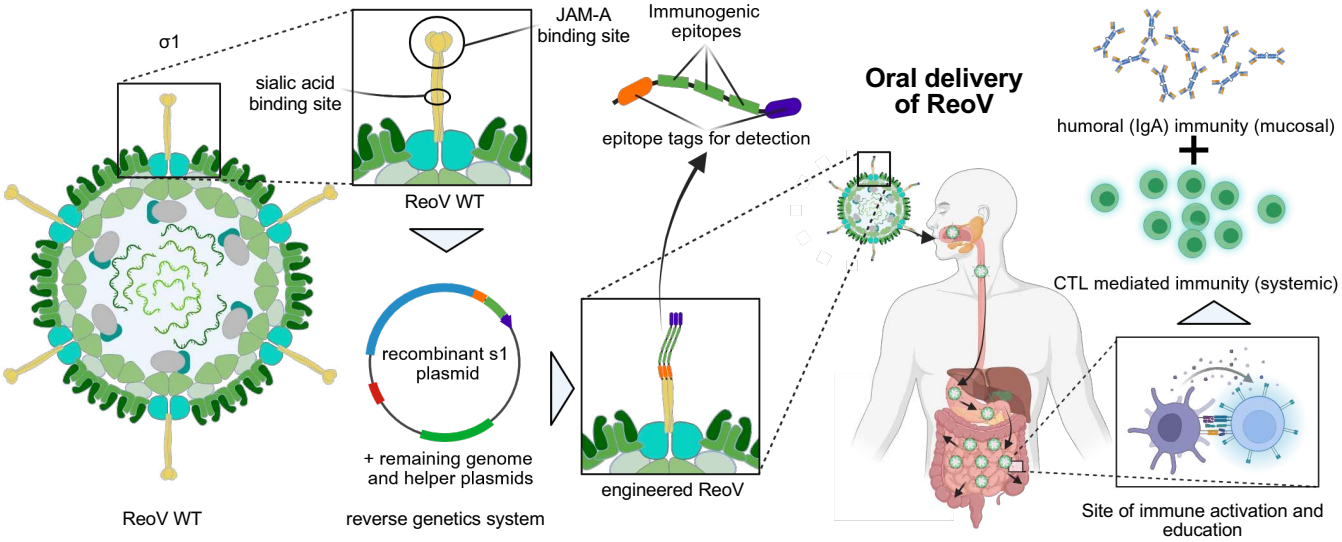
Virus replication is necessary for ReoV-OVA mediated cancer protection and is not affected by pre-exposure to virus. (**A**) Representative micrographs of L929 cells treated with either vehicle, active ReoV-OVA, or UV-Inactivated ReoV-OVA at an MOI of 10 show CPE only on cells treated with active virus. Scale bar = 400 μm. No virus was detected in vehicle and UV-Inactivated ReoV-OVA (NA) as indicated by results of a $TCID_{50}$ assay of the inoculum. (**B**) Validation of viral protein and transgene expression via immunoblotting. Infected cell lysates were probed by α-ReoV, α-FLAG, and α-Myc antibodies. (**C**) Immunization schedule. Mice were immunized PO with either vehicle, Active ReoV-OVA, or UV-Inactivated ReoV-OVA (n = 5) (1×10^9 $TCID_{50}$/dose, based on titers obtained before inactivation) as indicated. B16F10-OVA cells (2.5×10^5 cells) were injected IV and lungs were harvested on day 42. (**D**) Representative images of the lungs show significant differences in the amount of melanin positive tumour nodules. (**E**) Quantification of tumour burden as mean percentage of tumour surface area of the lungs. (**F**) Immunization schedule. Mice were immunized PO 6 times with ReoV WT (n = 5) on days 0, 2, 4, 13, 15, and 17 (1×10^9 $TCID_{50}$/dose). Then on days 26 and 33, vehicle or ReoV-OVA were injected PO (1×10^9 $TCID_{50}$/dose). On day 68, mice were euthanized and lungs were collected. (**G**) Representative images of the lungs show significant differences in the amount of melanin positive tumour nodules. (**H**) Quantification of tumour burden as mean percentage of tumour surface area of the lungs. All Data points represent mean ± SEM. ns; non-significant, *p < 0.05, **p < 0.01 and ***p < 0.001. CPE = cytopathic effect, IV = intravenous, MOI = multiplicity of infection, PO = per os, orally, ReoV = Reovirus, WT = wildtype.

Figure 5



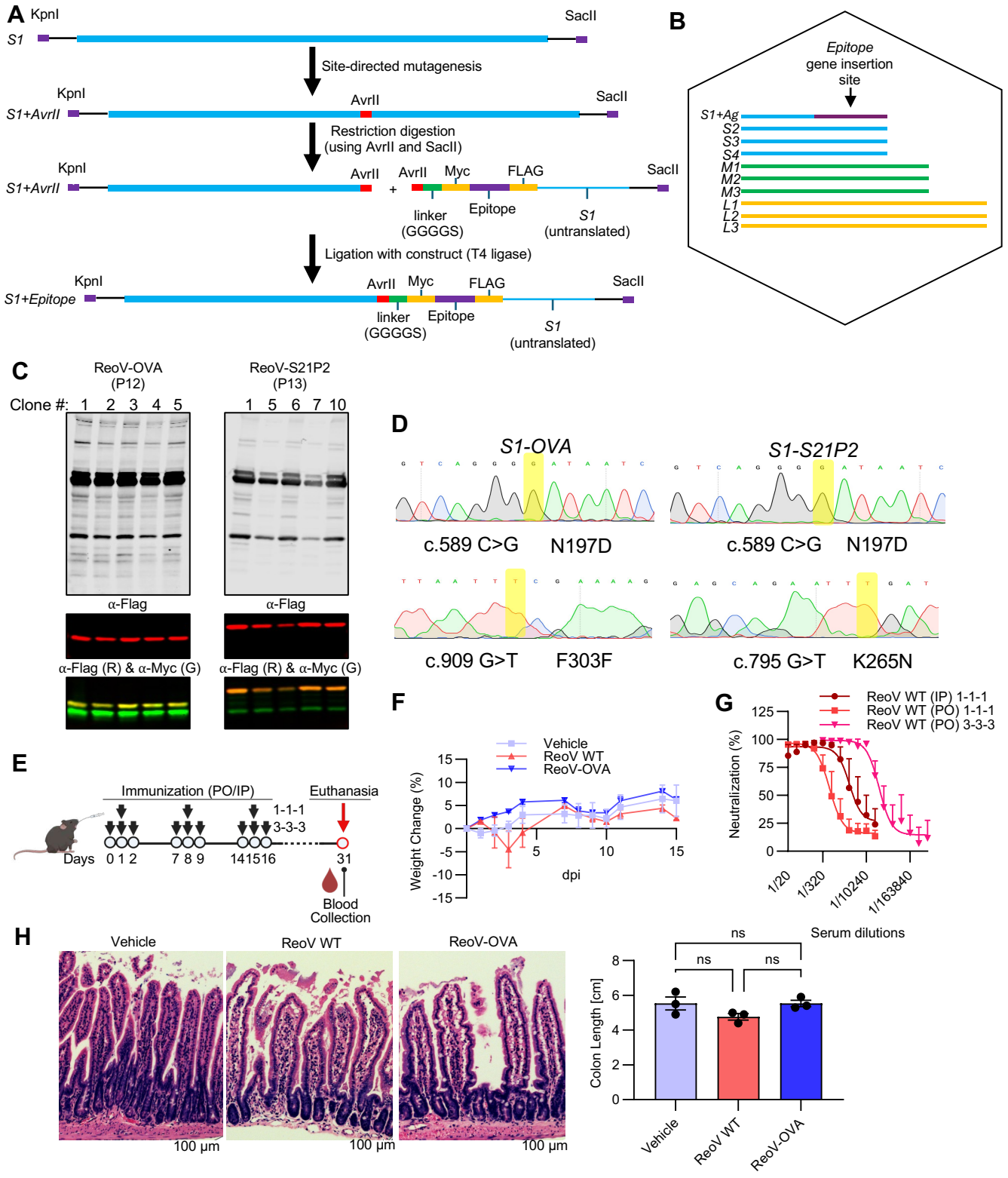
ReoV cancer interception is limited by antigen expression and synergizes with checkpoint inhibition. (**A**) Mice were immunized IP with ReoV WT (n = 5) or ReoV-OVA (*n* = 10, 1×10⁹ $TCID_{50}$/dose) as indicated. On day 14, B16F10 or B16F10-OVA cells (1×10⁶ cells) were implanted SC into the flank, and tumour volume was monitored, indicating antigen dependent delay in tumour progression conferring significant survival benefit. On day 40, mice (*n* = 7) receiving ReoV-OVA were rechallenged by SC implantation of MC38 (*n* = 3) or MC38-OVA (*n* = 4) cells (5×10⁴ cells) and tumour volume was monitored (**B+C**). (**D**) Quantification of TILs in B16F10 and B16F10-OVA tumours. Percentage of $CD45^+$ cells, and ratio of $CD8^+$:$CD4^+$ cells shows an increase of $CD8^+$ T cells in B16F10-OVA tumours vaccinated with ReoV-OVA. In an experiment like (**A**), 5×10⁴ B16F10 or B16F10-OVA cells were implanted and early B16F10-OVA tumours versus delayed ones show changes in melanin expression (**E**). (**F**) Immunoblotting for OVA expression shows significant downregulation. (**G**) Correlation between OVA expression and survival duration. (**H**) Comparison of delayed- and early-onset tumours in survival duration and level of OVA expression. (**I**) Immunoblotting for PD-L1 expression shows upregulation. (**J**) Combination with checkpoint inhibition: B16F10-OVA cells were implanted SC (day -14) and PO immunization as indicated (*n* = 8, 1×10⁹ $TCID_{50}$/dose) plus α-PD1 IP administration (200 µg) leads to a significant survival benefit for animals treated with a combination of ReoV-OVA and immune checkpoint inhibition. All Data points represent mean ± SEM. *P*-values for survival calculated by the Kaplan–Meier method followed by log-rank/mantel-Cox test. ns; non-significant, *p < 0.05, **p < 0.01 and ***p < 0.001. dpi = days post implantation, IP = intraperitoneal, IT = intratumoural, PO = orally, SC = subcutaneous, TILs = tumour infiltrating lymphocytes, WT = wildtype.

Figure 6



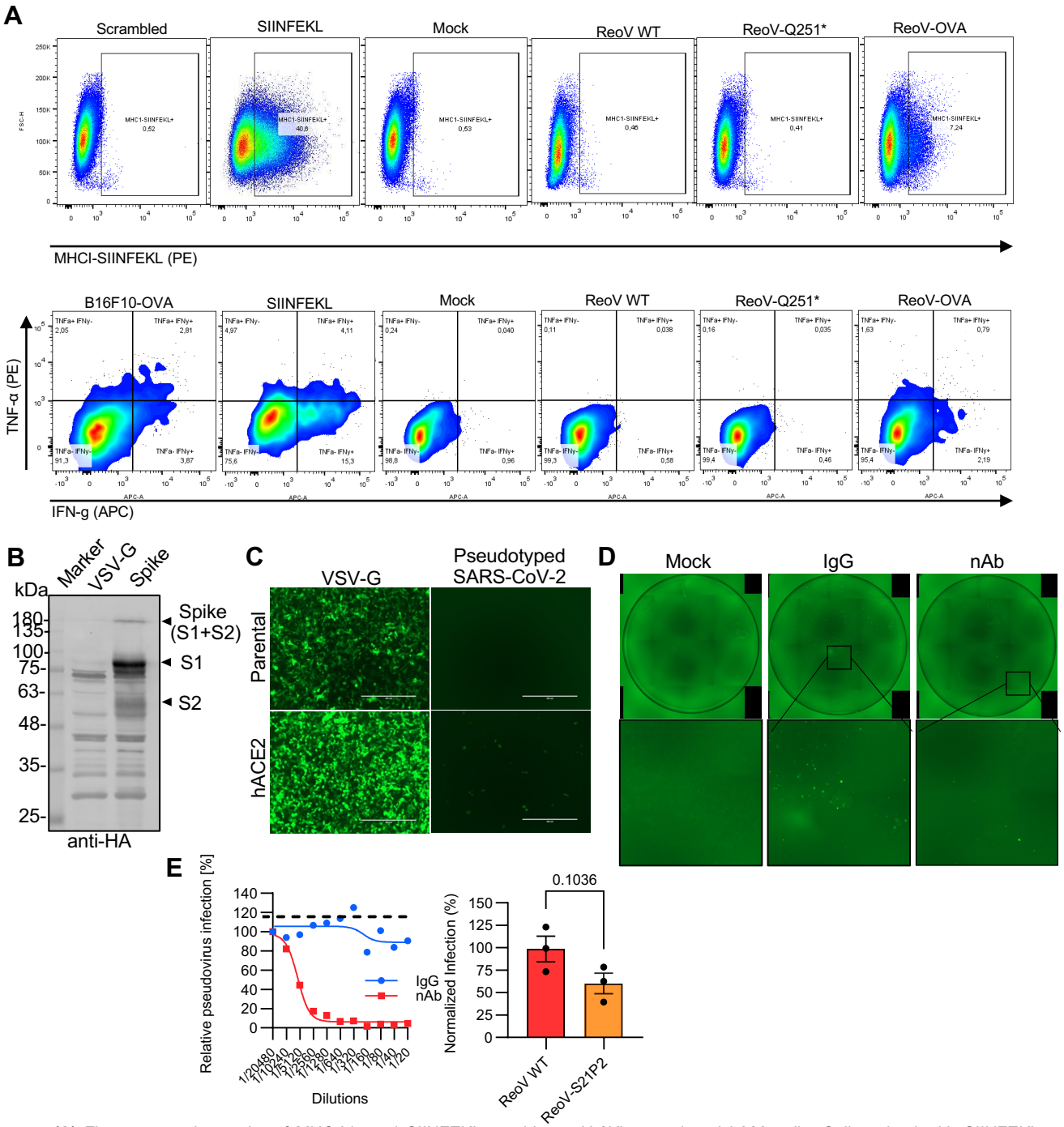
Design and mechanism of engineered reovirus for oral vaccination. Schematic overview of ReoV WT structure highlighting the σ1 protein, which mediates host cell attachment via SA and JAM-A binding sites. Using a reverse genetics system, immunogenic epitopes derived are genetically inserted into the S1 segment, along with epitope tags for detection, to generate an engineered reovirus. Following oral administration, the recombinant virus targets the, where it promotes immune activation and education. This results in the induction of both mucosal humoral immunity (IgA) and systemic cellular immunity, including CTL responses, contributing to robust antigen-specific immune protection. CTL= cytotoxic T lymphocyte, SA= Sialic Acid, JAM-A: Junctional adhesion molecule A, WT= Wildtype

Figure S1



(A) Schematic representation of the cloning strategy for the *S1+Epitope* construct using site-direct mutagenesis approach. **(B)** Schematic structure of recombinant reovirus. **(C)** Immunoblotting for reovirus, Flag- and Myc-tag expression in recombinant ReoV viruses, including ReoV-OVA, ReoV-S21P2 after several passages. **(D)** Genome sanger sequencing of reovirus *S1* genome. **(E)** C57BL/6 mice were immunized orally with vehicle, or ReoV WT, or ReoV-OVA (1×10^9 $TCID_{50}$/dose) (*n* = 3 in all groups). Oral administration of ReoV is well tolerated as demonstrated by no significant weight loss over time **(F). (G)** Oral Immunization with ReoV WT leads to neutralizing antibody response comparable to IP immunization as demonstrated by the neutralizing curve for the serum collected from mice immunized with ReoV WT via IP or PO, or an intensified oral regimen (3-3-3) (*n* = 3 per group). Percentage neutralization is plotted against 32-fold serial dilution of serum, starting at 1/20 base dilution. **(H)** No observable flattening or atrophy of the intestinal villi as demonstrated by H&E staining (left), and no change in the overall length of the colon (right).

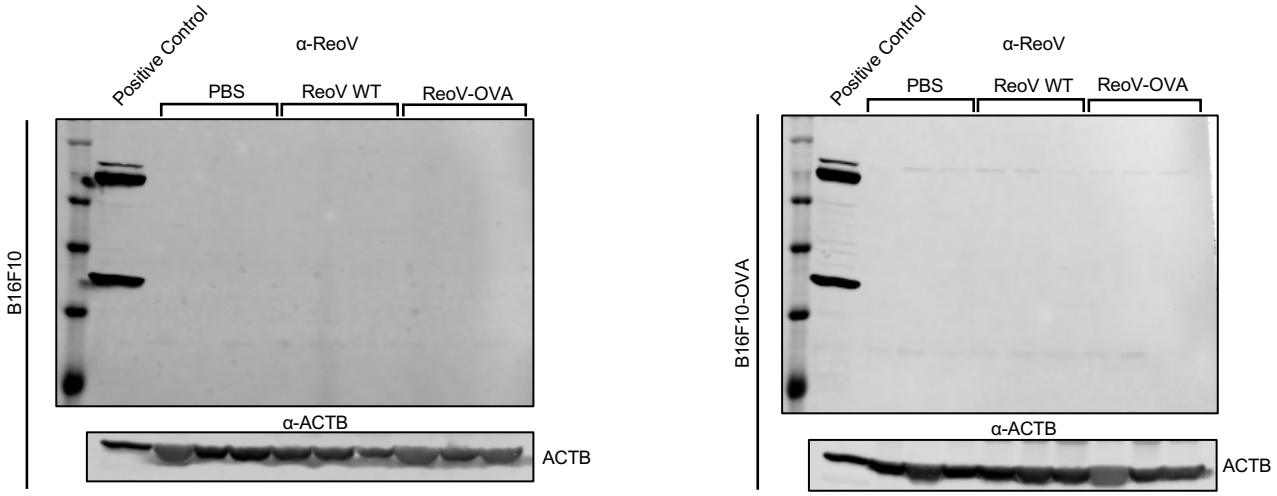
Figure S2



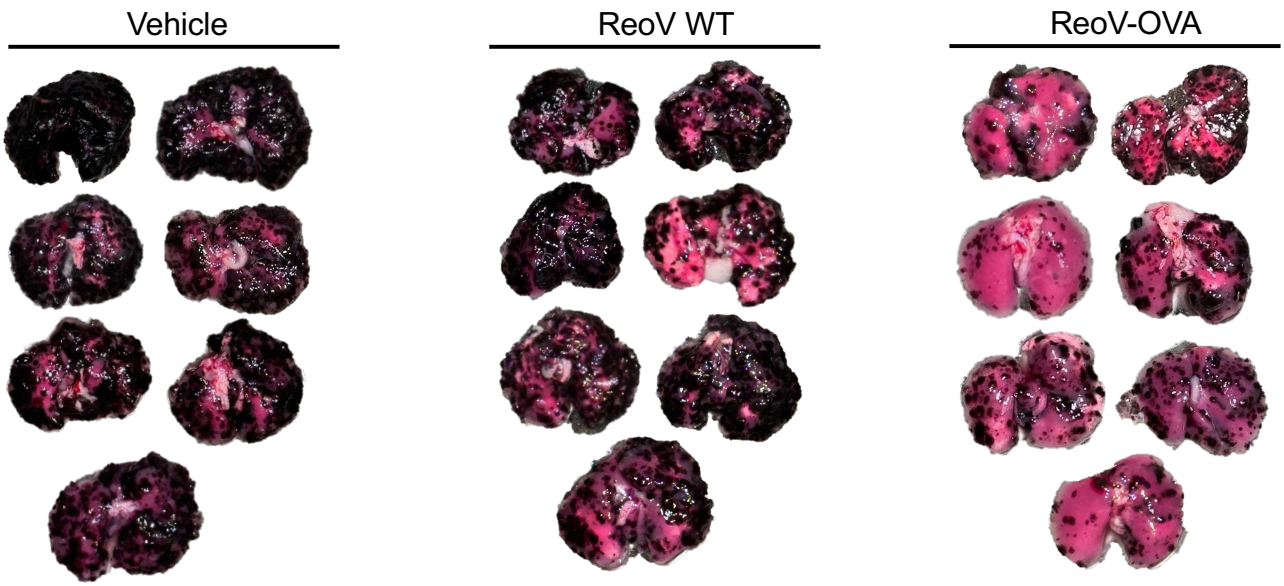
(A) Flow cytometric graphs of MHC-I-bound SIINFEKL peptide on H-2Kb transduced L929 cells. Cells pulsed with SIINFEKL peptide compared to scrambled peptide (Top). Flow cytometric graphs of activated $CD8^+$ cells by TNF-α and IFN-γ using OT-I mice splenocytes after co-culture with different variants of reovirus. **(B)** Western blot analysis of Spike protein expression probing for anti-HA antibody. **(C)** Fluorescence microscopy images showing the entry of VSV-G and SARS-CoV-2 pseudotypes into parental and hACE2-expressing cells, demonstrating hACE2-dependent entry for the SARS-CoV-2 pseudotype. **(D)** Neutralization assay showing a reduction in GFP-positive foci in cells treated with neutralizing antibodies (nAb) compared to Mock and IgG controls, confirming the specificity of the antibody-mediated inhibition. **(E)** Neutralization curve, with the nAb exhibiting a significant reduction in relative pseudovirus infection across serial dilutions compared to the IgG control (left), normalized infection percentages for ReoV WT and ReoV-S21P2 (right).

Figure S3:

A



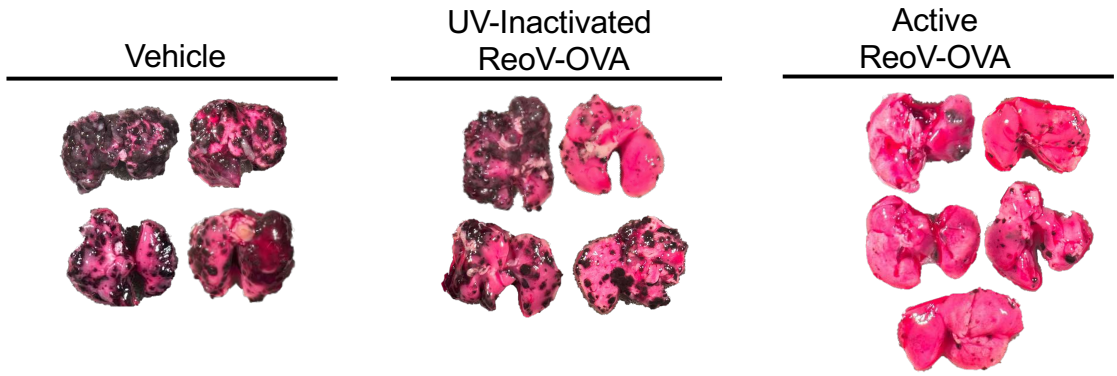
B



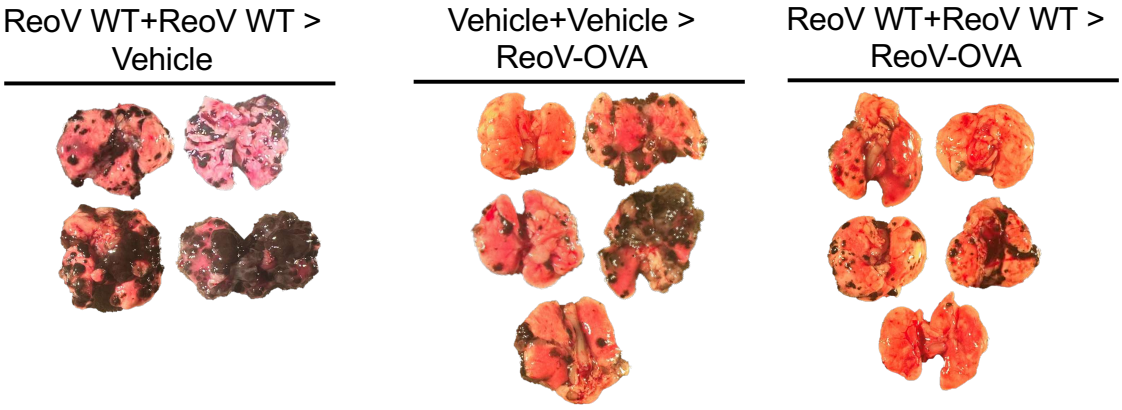
A) Representative blots resected tumours of mice (B16F10 **Left** and B16F10-OVA **Right**) showing that there is no viral particle detected within TME. **B)** Images of the all lungs showing marked reduction of metastasized tumour nodules in lungs vaccinated with ReoV-OVA compared to vehicle and ReoV WT.

Figure S4:

A

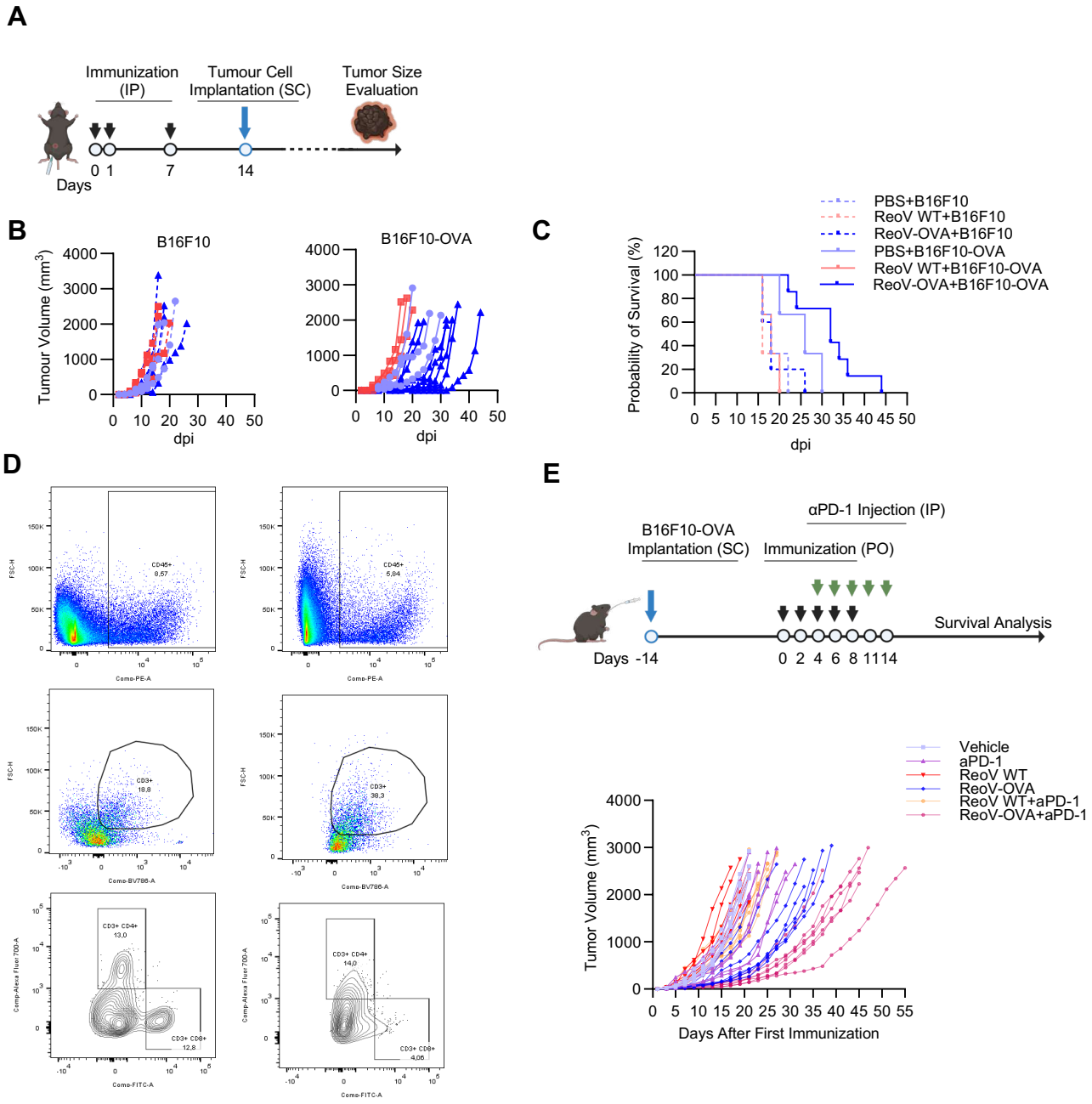


B



A) Images of the all lungs in UV model. Mice immunized with Active ReoV-OVA showed less tumour nodules compared to those immunized with UV-inactivated ReoV-OVA indicating that viral replication is vital for inducing antitumour effect by the vaccine. **(B)** Images of all the lungs. Mice with or without pre-exposure to ReoV WT showed no difference in lungs' tumour nodules if they receive the ReoV-OVA vaccine.

Figure S5:



(A) Immunization schedule. Mice were immunized IP with either PBS, ReoV WT, or ReoV-OVA ($TCID_{50}$/dose) on days 0, 1, and 7 and 5×10^4 cells (either B16F10 or B16F10-OVA) were implanted SC on day 14 into the flank and tumour development and survival were monitored. **(B)** Mice implanted with B16F10 cells, developed tumour faster regardless of the type of the vaccine injected (**Left**); however, the mice immunized with ReoV-OVA and then implanted with B16F10-OVA cells developed the tumour slower compared to those mice immunize with PBS or ReoV WT **(Right)**. **(C)** The mice immunized with ReoV-OVA and had B16F10-OAV tumour had better survival rate compared to other groups. **(D)** Flow cytometric graphs of TILs in TME. **(E)** Immunization schedule for combination therapy: B16F10-OVA cells were implanted SC (day -14) and PO immunization as indicated (n = 8, 1×10^9 $TCID_{50}$/dose) plus α-PD1 IP administration (200 µg). **(E)** Mice immunized with ReoV-OVA (as monotherapy or in combination with α-PD1) developed tumour in a slower pace compared to other groups. TME= Tumour microenvironment

Tabel S1

Primers used in PCR

Target Gene	**Sequence 5'-3'**
S1	FWD: GATGGATCCTCGCCTACGTG REV: TCATCGAGTCCCTGGGTGAT
RBD Spike	FWD: CAACTGAGCAAAGTTACGTGAGGGTACAACCTACGGAATC REV: ATGAAATGCCCCAGTGCCGCGGGGTGGTCTGACCTCAAAAATTGACGCATTTATTCTTCAC
S1 Sequencing	FWD: GCTATTGGTCGGATGGATCCTCGC REV: GATCCTCACGTGAAACTACGCGGGTA

Table S2

Antibodies used flow cytometry

Target Antibody	Conjugate	Manufacturer	Cat. #
TruStain FcX (anti-mouse CD16/32)		BioLegend	101320
Zombie Violet Fixable Viability Kit	BV421 Equivalent	BioLegend	423114
Anti-mouse IFN-ɣ	APC	BioLegend	505810
Anti-mouse TNF-α	PE	BioLegend	506306
Anti-mouse CD3	BV785	BioLegend	100231
Anti-mouse CD4	AF700	BioLegend	100536
Anti-mouse CD8	FITC	BioLegend	100706
Anti-mouse CD45	PE	BioLegend	103106
Anti-mouse H-2Kb bound to SIINFEKL	PE	BioLegend	141604